

## Electronic Supplementary Information

### **Contact with soil impacts ferrihydrite and lepidocrocite transformations during redox cycling in a paddy soil**

*Katrin Schulz<sup>1</sup>, Luiza Notini<sup>1</sup>, Andrew R. C. Grigg<sup>1</sup>, L. Joëlle Kubeneck<sup>1</sup>, Worachart Wisawapipat<sup>2</sup>,  
Laurel K. ThomasArrigo<sup>1,3</sup>, Ruben Kretzschmar<sup>1</sup>*

<sup>1</sup> Soil Chemistry Group, Institute of Biogeochemistry and Pollutant Dynamics, Department of Environmental Systems Science, ETH Zurich, Universitätstrasse 16, CHN, CH-8092 Zurich, Switzerland.

<sup>2</sup> Soil Chemistry and Biogeochemistry Group, Department of Soil Science, Faculty of Agriculture, Kasetsart University, Bangkok 10900, Thailand

<sup>3</sup> Environmental Chemistry Group, Institute of Chemistry, University of Neuchâtel, Avenue de Bellevaux 51, 2000, Neuchatel, Switzerland.

*(Contains 23 figures and 13 tables)*

## **Contents**

S1. Soil characterization .....	S3
S2. Characterization of initial <sup>NA</sup> Fe-minerals and <sup>57</sup> Fe-mineral-soil mixes .....	S5
S3. Experimental setup and sampling .....	S8
Mesocosm setup details.....	S8
Comparison of oxic and anoxic drying of mesh bags .....	S10
S4. Soil conditions during the incubation.....	S11
S5. Additional porewater data .....	S12
S6. Elemental composition of <sup>NA</sup> Fe-minerals after incubation.....	S13
S7. X-ray diffraction.....	S14
Method details .....	S14
Mineral fractions in <sup>NA</sup> Fe-mineral samples.....	S15
Fitting parameters .....	S17
Magnetite stoichiometry.....	S18
S8. Fe K-edge X-ray absorption spectroscopy .....	S19
Measurement details and fitting.....	S19
Additional data from Fe K-edge XAS of <sup>NA</sup> Fe-mineral samples.....	S20

S9. Aqua regia digestion.....	S22
S10. Sequential iron extractions .....	S26
S11. Mössbauer spectroscopy.....	S28
Sample preparation and measurement details.....	S28
Magnetite fitting in <sup>NA</sup> Fe-mineral samples (permanently flooded mesocosm) .....	S29
Additional data (77 K and 295 K).....	S30
Collapsed feature in Mössbauer spectra.....	S32
Fitting parameters (77 K) of <sup>57</sup> Fe-mineral-soil mixes.....	S34
Fitting parameters (5 K) of <sup>57</sup> Fe-mineral-soil mixes.....	S36
Fitting parameters (5 K) of <sup>NA</sup> Fe-mineral samples.....	S41
S12. Comparison of iron mineral fractions determined by different methods .....	S43
References.....	S44

### S1. Soil characterization

Element contents and the texture of the soil are given in Table S1. The Mössbauer spectra of the initial soil collected at 77 K and 5 K are shown in Figure S1. Due to the low Fe content of the soil (0.3 %), Mössbauer spectra show high spectral noise despite long measurement times (>1 week per temperature). With the high spectral noise, the spectral features were not as clear and thus the fitting was challenging. Therefore, all fitting parameters had to be fit individually and were then fixed. The parameters for sextet S1 in the 77 K spectrum (center shift, CS = 0.44 mm s<sup>-1</sup>, quadrupole shift,  $\epsilon$  = -0.11 mm s<sup>-1</sup>, hyperfine field, H = 49.70 T,  $\sigma_H$  = 2.85 T) agree with values reported for goethite.<sup>1</sup> Parameters for doublet D1 (CS = 0.45 mm s<sup>-1</sup>, QS = 0.83 mm s<sup>-1</sup>,  $\sigma_{QS}$  = 0.48 mm s<sup>-1</sup>) and D2 (CS = 1.2 mm s<sup>-1</sup>, quadrupole splitting, QS = 2.36 mm s<sup>-1</sup>,  $\sigma_{QS}$  = 0.72 mm s<sup>-1</sup>) agree with parameters for Fe(III) and Fe(II), respectively.<sup>1</sup> At 5 K, an additional sextet (S2) was necessary to fit the spectrum (CS = 0.47 mm s<sup>-1</sup>,  $\epsilon$  = -0.007 mm s<sup>-1</sup>, H = 48.84 T,  $\sigma_H$  = 2.74 T), with parameters similar to those reported for ferrihydrite.<sup>2</sup> Collectively, the Mössbauer spectra indicate that ferrihydrite and goethite were the main Fe-mineral phases in the soil, combined with silicate or organic matter associated Fe(III) and small amounts of solid-associated Fe(II). This generally agrees with results from sequential Fe extractions (Figure S2), where 60% of extractable Fe was extracted with the fraction of reducible Fe oxides, such as goethite (citrate dithionate bicarbonate).<sup>3</sup> Smaller portions of Fe were extracted with fractions of easily reducible Fe oxides, such as ferrihydrite (Hydroxylamine hydrochloric acid, 11%),<sup>3</sup> Fe in carbonates (sodium acetate, 14%),<sup>3</sup> and Fe in recalcitrant Fe oxides (Ammonium oxalate, 12%).<sup>3</sup> Residual Fe may be associated with clay minerals. Relative to the total Fe in the soil (3.3 g kg<sup>-1</sup>), the extractable reactive Fe fraction was 24%. Method details on the sequential Fe extractions are presented in ESI Section S10.

**Table S1:** Characterization of the rice paddy soil (0-15 cm depth) included in this experiment, with element concentrations measured in dried, sieved (<2 mm) and milled soil by X-ray fluorescence spectroscopy (XRF), an elemental analyzer (EA) or after total digestion with hydrofluoric acid (HF), and the texture determined on dried and sieved (<2 mm) soil.

<b>Element concentrations</b>	Fe	3.3 g kg <sup>-1</sup>	XRF
	Si	417.4 g kg <sup>-1</sup>	XRF
	Al	14.0 g kg <sup>-1</sup>	XRF
	C	4.0 g kg <sup>-1</sup>	EA
	N	0.5 g kg <sup>-1</sup>	EA
	P	0.08 g kg <sup>-1</sup>	HF
<b>Texture</b>	Sand	84.8%	
	Silt	12.6%	
	Clay	2.6%	

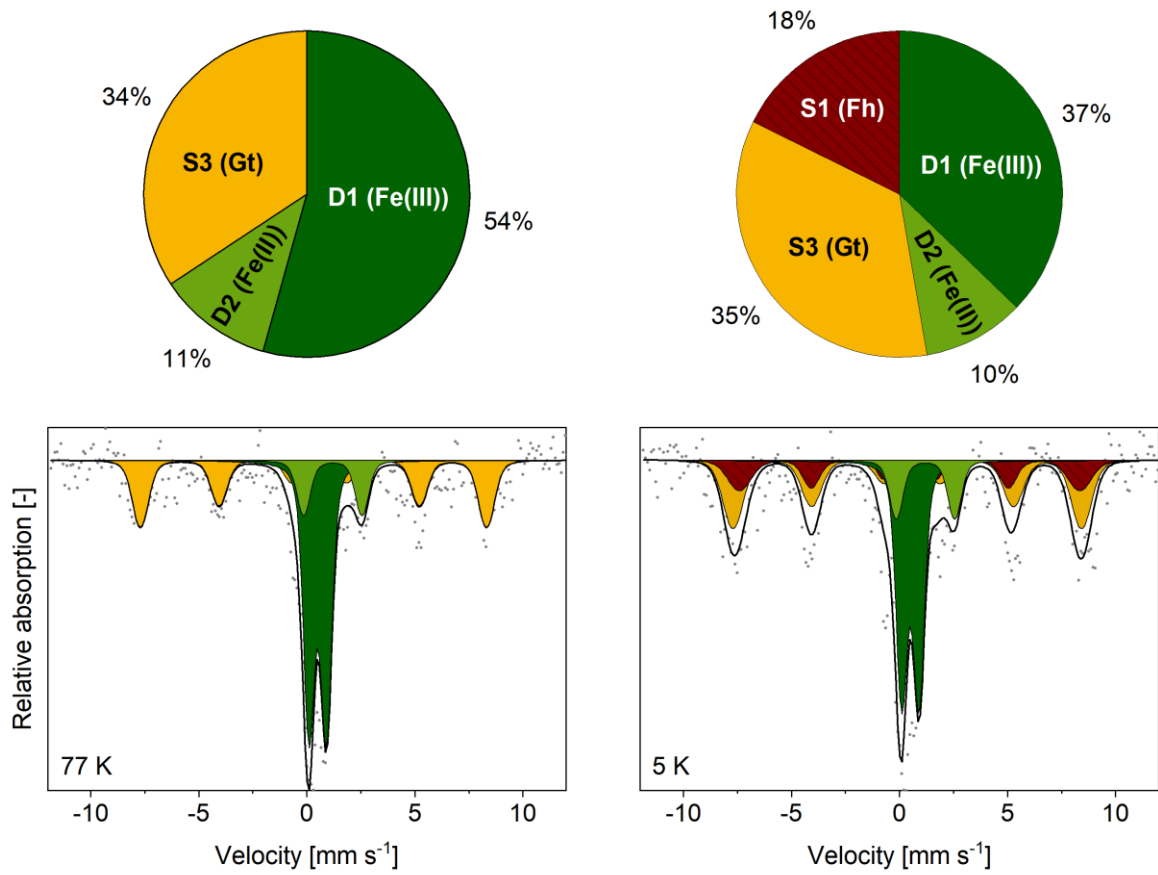


**Figure S1:** Mössbauer spectra of the rice paddy soil used in this experiment with respective spectral areas of fitted mineral fractions (pie charts), measured at 77 K (left) and 5 K (right). The colors and labels in the pie charts correspond to the colors of the fitting components in the Mössbauer spectra. Abbreviations: Fh = ferrihydrite, Gt = goethite, S = sextet, D = doublet.

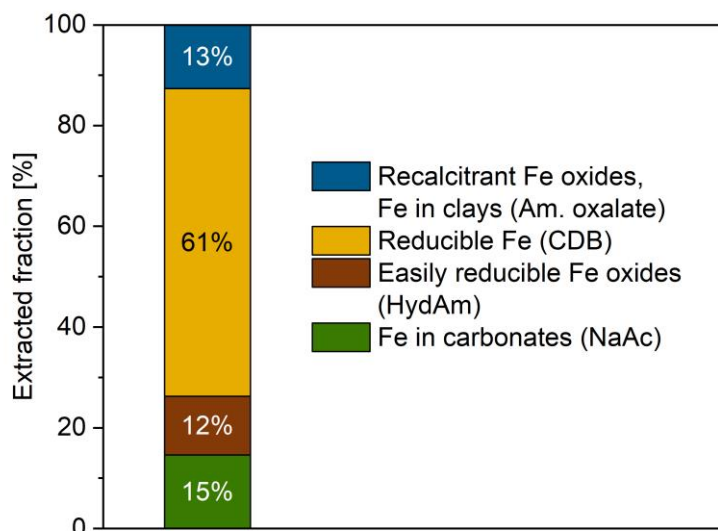


**Figure S2:** Sequential iron extraction results for the rice paddy soil used in this experiment with five extraction steps: (1) Calcium chloride ( $\text{CaCl}_2$ ), (2) Sodium acetate (NaAc), (3) Hydroxylamine hydrochloric acid (HydAm), (4) Citrate dithionite bicarbonate (CDB), (5) Ammonium oxalate (Oxalate). Details of extraction steps are found in Section S10.

## S2. Characterization of initial $^{57}\text{Fe}$ -minerals and $^{57}\text{Fe}$ -mineral-soil mixes

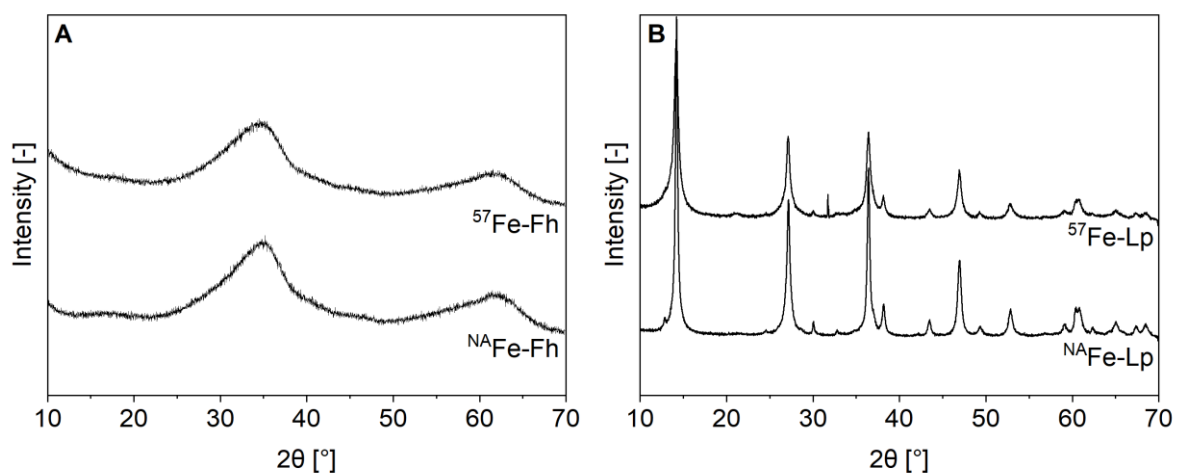


**Figure S3:** X-ray diffraction patterns of initial ferrihydrites (A) and lepidocrocites (B) with natural abundance Fe ( $^{57}\text{Fe}$ -Fh,  $^{57}\text{Fe}$ -Lp) and isotopically labeled with  $^{57}\text{Fe}$  ( $^{57}\text{Fe}$ -Fh,  $^{57}\text{Fe}$ -Lp). Abbreviations: Fh = ferrihydrite, Lp = lepidocrocite.

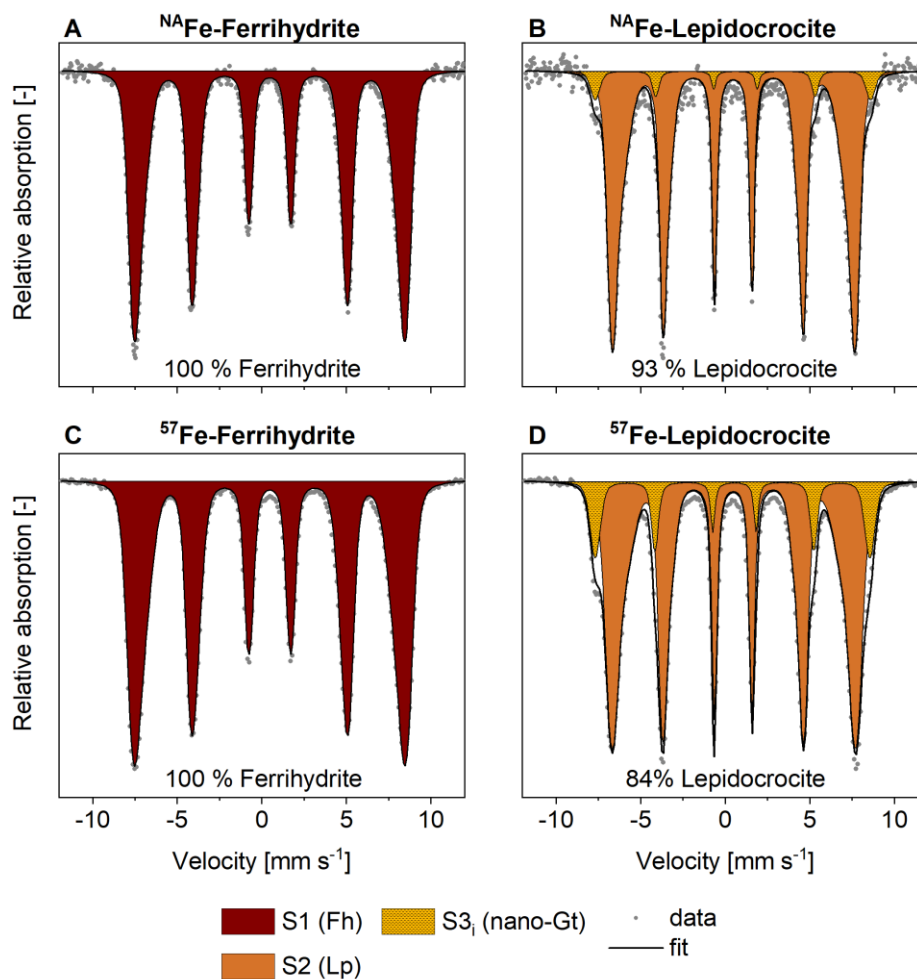


**Figure S4:** Mössbauer spectra (5 K) of initial  $^{54}\text{Fe}$ -ferrihydrate (A),  $^{54}\text{Fe}$ -lepidocrocite (B),  $^{57}\text{Fe}$ -ferrihydrate (C) and  $^{57}\text{Fe}$ -lepidocrocite (D). Fitting parameters are presented in Table S2, the fits are discussed below. Abbreviations: S = sextet, Fh = ferrihydrate, Lp = lepidocrocite, Gt = goethite.

The Mössbauer spectra collected at 5 K from initial  $^{54}\text{Fe}$ -ferrihydrate ( $^{54}\text{Fe}$ -Fh) and  $^{54}\text{Fe}$ -lepidocrocite ( $^{54}\text{Fe}$ -Lp) minerals and from  $^{57}\text{Fe}$ -ferrihydrate ( $^{57}\text{Fe}$ -Fh) and  $^{57}\text{Fe}$ -lepidocrocite ( $^{57}\text{Fe}$ -Lp)-soil mixes are presented in Figure S4 with fitting parameters reported in Table S2. The spectra collected at 5 K from the initial  $^{54}\text{Fe}$ -Fh and  $^{57}\text{Fe}$ -Fh-soil mix show a sextet (S1) with parameters ( $CS = 0.48 \text{ mm s}^{-1}$ ,  $\varepsilon = -0.004 \text{ mm s}^{-1}$ ,  $H = 49 \text{ T}$ ) consistent with ferrihydrate.<sup>2</sup> The spectra of the initial  $^{54}\text{Fe}$ -Lp and the  $^{57}\text{Fe}$ -Lp-soil mix contain a sextet (S2) with parameters ( $CS = 0.49 \text{ mm s}^{-1}$ ,  $\varepsilon = 0.02 \text{ mm s}^{-1}$ ,  $H = 43 \text{ T}$ ) consistent with parameters reported for lepidocrocite.<sup>4</sup> However, a second sextet (S3) was present in the spectrum of the  $^{54}\text{Fe}$ -Lp (7%) and the  $^{57}\text{Fe}$ -Lp-soil mix (16%) ( $CS = 0.51 \text{ mm s}^{-1}$ ,  $\varepsilon = -0.06 \text{ mm s}^{-1}$ ,  $H = 50.45 \text{ T}$ ). Considering that the  $\varepsilon$  of this sextet is smaller compared to typical values reported for goethite ( $-0.12 \text{ mm s}^{-1}$ , ref 1) and no goethite peaks were visible in X-ray diffraction patterns (Figure S3), we expect that goethite in these samples was nano-crystalline.<sup>1</sup>

**Table S2:** Mössbauer fitting parameters for spectra collected at 5 K from initial <sup>54</sup>Fe-ferrihydrite and <sup>54</sup>Fe-lepidocrocite samples without soil, and for <sup>57</sup>Fe-ferrihydrite and <sup>57</sup>Fe-lepidocrocite-soil mixes. The values corresponding to the use of multiple components for parameters are marked in brown.

Sample	Component	CS <sup>a</sup> [mm s <sup>-1</sup> ]	ε <sup>b</sup> [mm s <sup>-1</sup> ]	σ <sub>ε</sub> <sup>c</sup> [mm s <sup>-1</sup> ]	H <sup>d</sup> [T]	σ <sub>H</sub> <sup>c</sup> [T]	Area [%]	Red. χ <sup>2e</sup>
<sup>54</sup> Fe-Fh	S1 – Fh	0.48	-0.004	0.16	49.05	1.57	100	1.17
	H1				49.95	1.29		
	H2				46.83	2.25		
	Frac H2				29%			
<sup>57</sup> Fe-Fh-soil mix	S1 – Fh	0.47	-0.007	0.19	48.84	2.74	100	2.90
<sup>54</sup> Fe-Lp	S2 – Lp	0.49	0.01	-	43.29	2.16	93.2	1.02
	H1				44.64	1.2*		
	H2				42.00	3.1*		
	Frac H2				51%			
	S3 – Gt	0.53	-0.07	-	50.52	1.3	6.8	
<sup>57</sup> Fe-Lp-soil mix	S2 – Lp	0.49	0.02	-	43.40	2.28	84.4	1.43
	H1				44.82	2.00*		
	H2				39.76	3.00*		
	Frac H2				28%			
	S3 - Gt	0.49	-0.05	-	50.37	1.5*	15.6	

<sup>a</sup> CS, Center shift;<sup>b</sup> ε, Quadrupole shift;<sup>c</sup> σ, standard deviation of ε or H;<sup>d</sup> H, Hyperfine field;<sup>e</sup> Reduced χ<sup>2</sup>, goodness of fit;

\* Indicates values that were fixed during the fitting process.

Abbreviations: w = week, Fh = ferrihydrite, Lp = lepidocrocite, Gt = goethite, S = sextet.

### S3. Experimental setup and sampling

#### Mesocosm setup details

The soil mesocosms were made from two rectangular plastic boxes (polypropylene, length x width x height = 37.6 x 26 x 28.3 cm, volume = 20 L), which were stacked, resulting in a gap of ~3 cm between the bottoms of the boxes (Figure S5). A drainage port (diameter ~1 cm) was installed on the lower box and equipped with a valve. In the upper box, five holes of ~0.5 cm were punched into the bottom to allow soil drainage through the bottom of the mesocosms. To reduce the loss of soil during drainage, a mesh fabric (PETE, pore size = 105  $\mu\text{m}$ ; SEFAR, Switzerland) was placed on the bottom of each upper box.

A ~1 cm thick sand layer (grain size 0.1-0.5 mm, acid-washed, 1.5 kg sand) was created in the upper box of each mesocosm to facilitate the drainage process. On top of the sand layer, 12 kg of dry soil was spread, without compacting the soil, resulting in a soil depth of ~12 cm. The packing of the mesocosms resulted in a slight horizontal layering of coarse and fine soil particles, visible through slight color differences. Therefore, the soil was gently homogenized by hand after packing, without affecting the sand layer. Pictures of the sample holders containing the mesh bags before the insertion into the soil and after the sampling are shown in Figure S6.

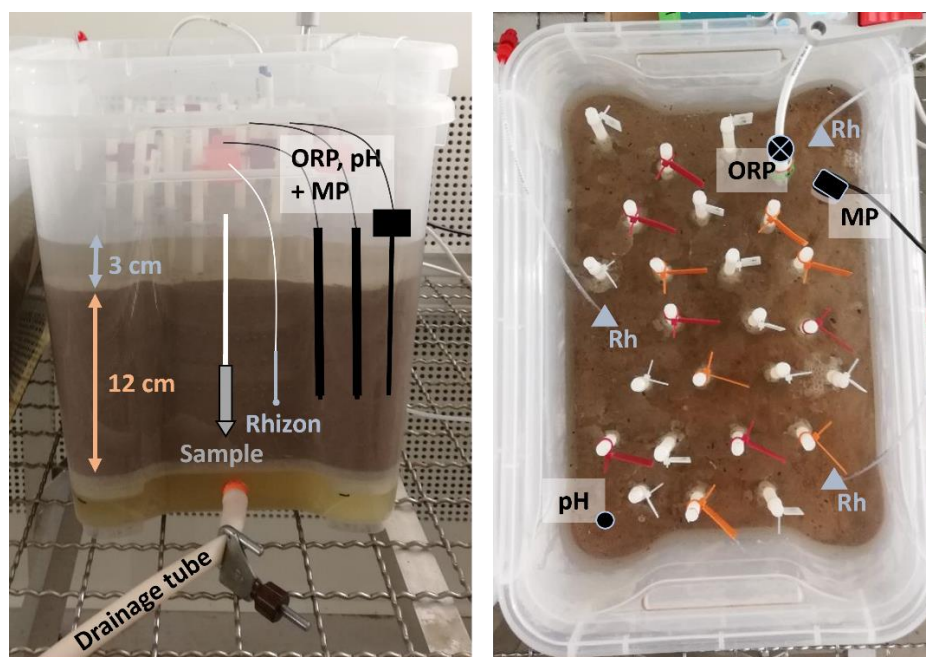
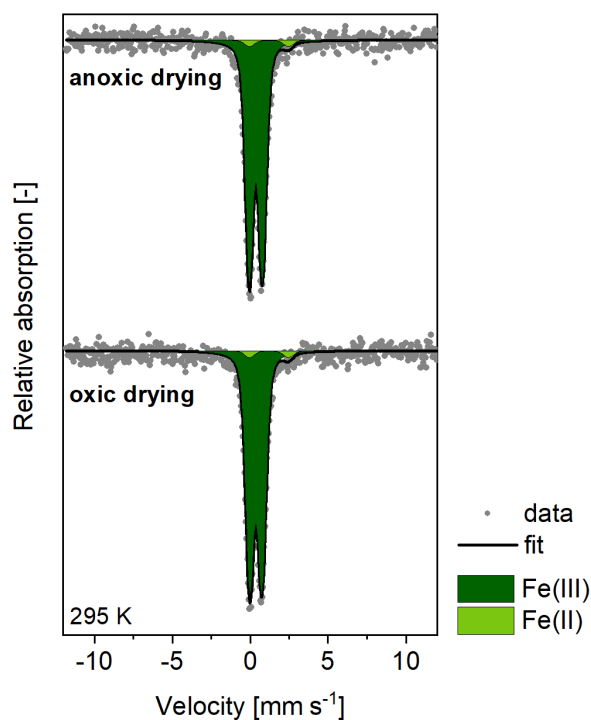


**Figure S5:** Experimental setup showing stacked plastic boxes (L x W x H = 37.6 x 26 x 28.3 cm ) with flooded soil (left), and the position of samples with colored marks (red =  $^{57}\text{Fe}$ -Fh, orange =  $^{57}\text{Fe}$ -Lp, white =  $^{54}\text{Fe}$ -mineral samples), porewater samplers (Rhizon/Rh) and sensors for measuring the oxidation-reduction potential (ORP), pH and matric potential (MP) (right).



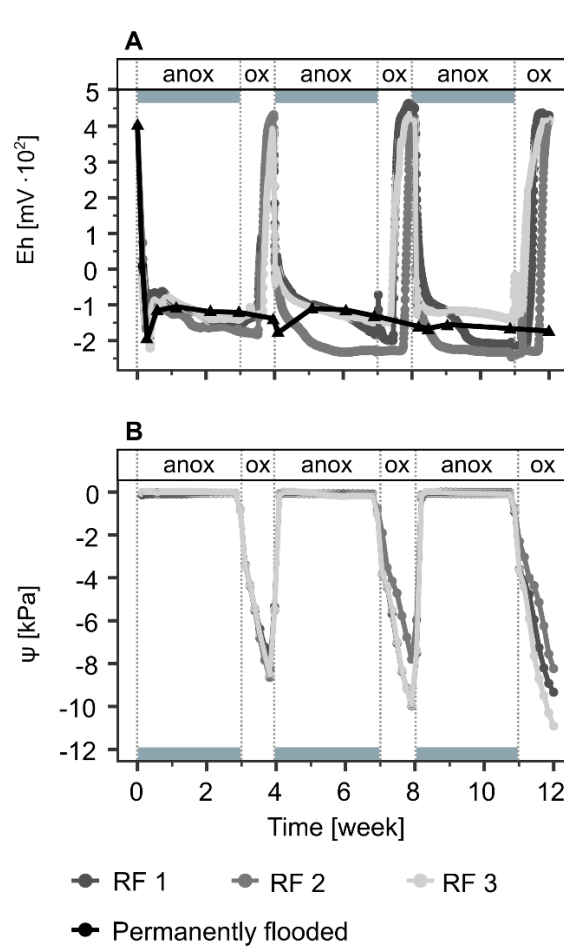
**Figure S6:** Sample holder without mesh bag (left, length = 5 cm, diameter = 1 cm) and during the sampling after the oxic sampling in redox cycle I at 4 weeks (right).

## Comparison of oxic and anoxic drying of mesh bags

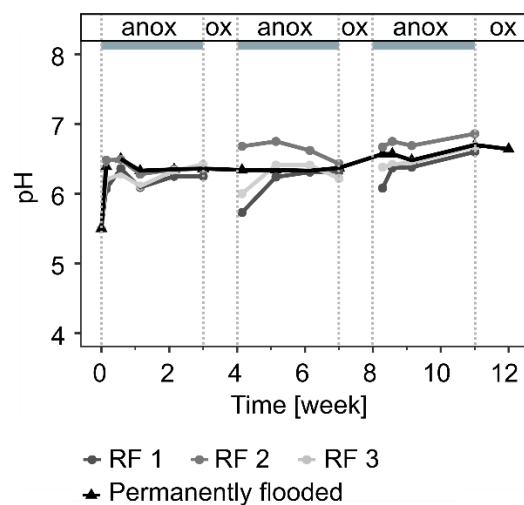


**Figure S7:** Mössbauer spectra (295 K) of  $^{57}\text{Fe}$ -ferrihydrite-soil mixes dried under oxic (A) or anoxic (B) conditions after the exposure to one soil redox cycle (3 weeks anoxic, 1 week oxic). Averaged fitting parameters for the Fe(III) doublets in the two samples were: Center shift =  $0.36 \text{ mm s}^{-1}$ , quadrupole splitting (QS) =  $0.81 \text{ mm s}^{-1}$  and  $\sigma_{\text{QS}} = 0.40 \text{ mm s}^{-1}$ . Fitting parameters for Fe(II) doublet were: Center shift =  $1.20 \text{ mm s}^{-1}$ , quadrupole splitting (QS) =  $2.50 \text{ mm s}^{-1}$  and  $\sigma_{\text{QS}} = 0.5 \text{ mm s}^{-1}$  and had to be fixed for the fit due to the small contribution of this doublet to the spectral area. Based on the similar Fe(II) fractions in the spectra from the two samples, we are confident that no additional oxidation occurred during the oxic drying of samples from oxic periods.

S4. Soil conditions during the incubation

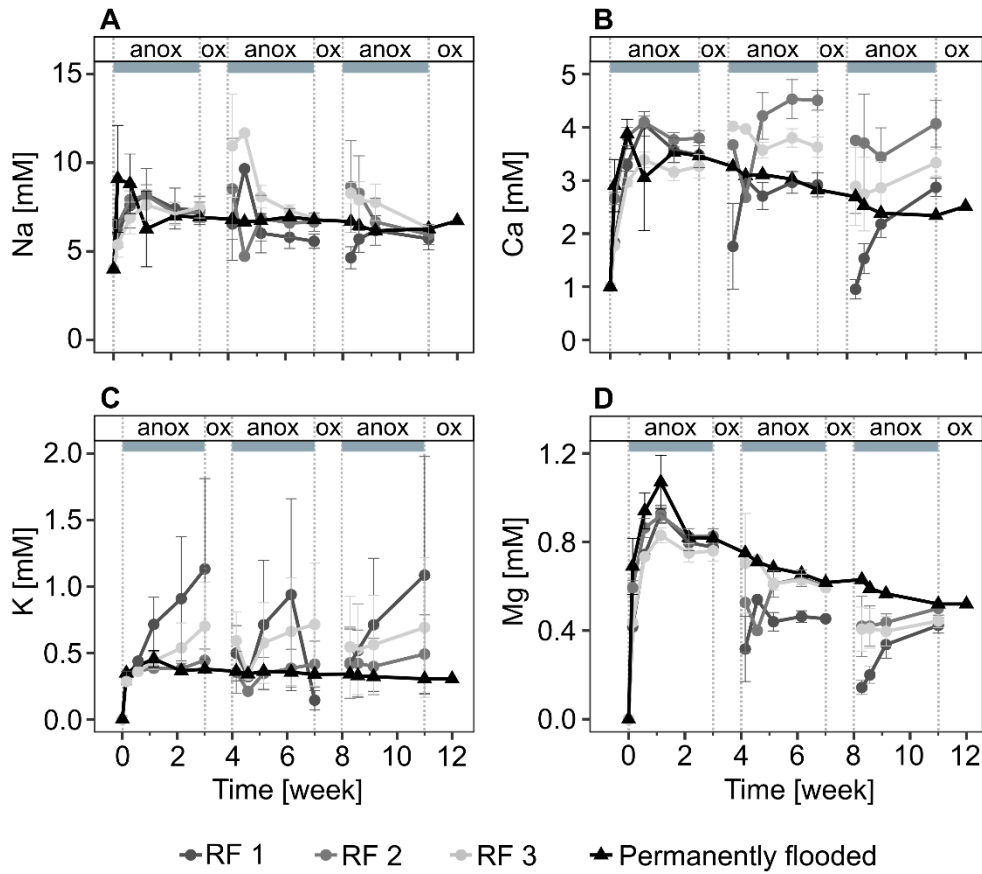


**Figure S8:** Redox potential (Eh, A) in the redox fluctuating (RF 1-3) and the permanently flooded mesocosms, and matric potentials ( $\psi$ ) in the redox fluctuating mesocosms. Labels above the data indicate anoxic (anox, grey boxes) and oxic (ox) periods, as induced by flooding and drainage of the soil.

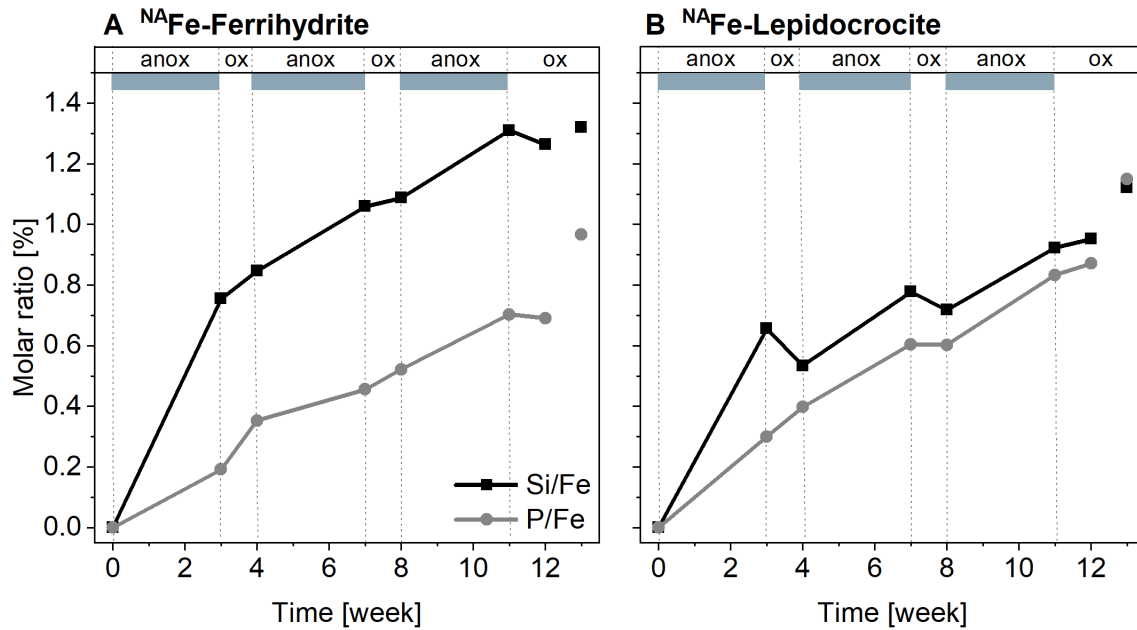


**Figure S9:** Soil porewater pH values before (initial soil, pH in 0.1 mM  $\text{CaCl}_2$ , timepoint = 0) and during the 12-week incubation of the experimental rice paddy soil in the three redox fluctuating (RF 1-3) and the permanently flooded mesocosm. Labels above grey boxes indicate anoxic (anox, grey boxes) and oxic (ox) periods.

S5. Additional porewater data



**Figure S10:** Dissolved concentrations of sodium (Na), calcium (Ca), potassium (K), and magnesium (Mg) in the porewater of soils in the redox fluctuating (RF 1-3) and the permanently flooded mesocosms. Labels above grey boxes indicate anoxic (anox, grey boxes) and oxic (ox) periods. Error bars show the standard error of triplicate pore water samplers in each mesocosm.

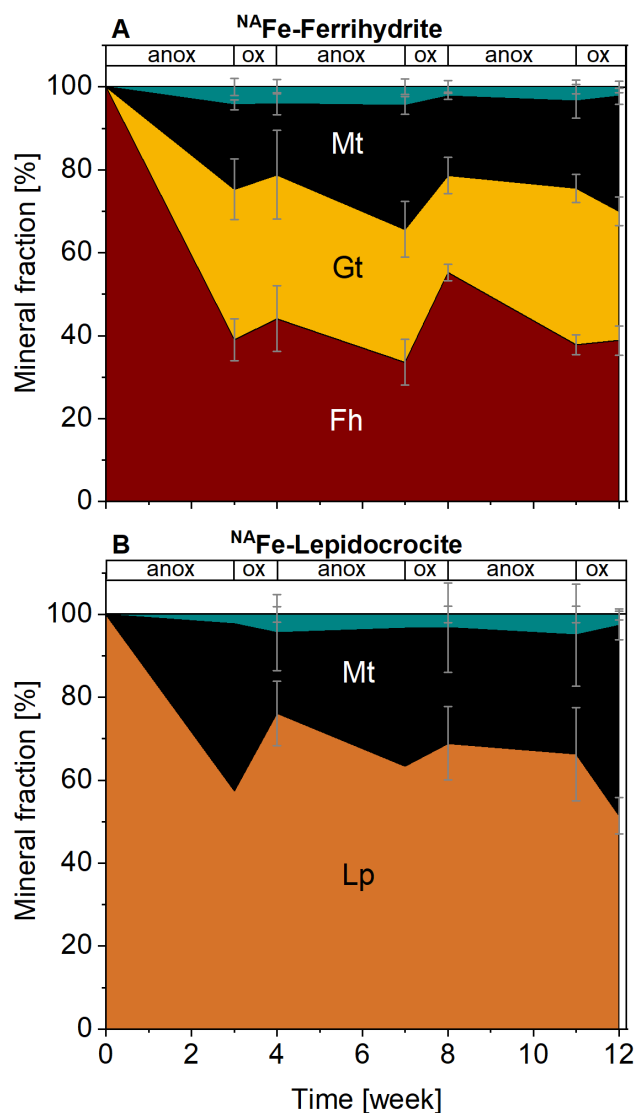
S6. Elemental composition of  $^{54}\text{Fe}$ -minerals after incubation

**Figure S11:** Molar ratios of P/Fe and Si/Fe in  $^{54}\text{Fe}$ -ferrihydrate and  $^{54}\text{Fe}$ -lepidocrocite samples before and during the incubation in the redox fluctuating mesocosms (line and symbol) and in the permanently flooded mesocosm (single symbols) for 12 weeks. Element contents were measured by ICP-OES after acid dissolution of minerals. Labels above grey boxes indicate anoxic (anox, grey boxes) and oxic (ox) periods.

## S7. X-ray diffraction

### Method details

For X-ray diffraction (XRD) measurements, ~2 mg dried sample material was resuspended in ~30  $\mu\text{L}$  ethanol and pipetted onto a zero-background polished silicon wafer (Sil'tronix Silicon Technologies, France). The XRD measurements were conducted using  $\text{Cu K}\alpha_1$  and  $\text{Cu K}\alpha_2$  radiation ( $\lambda_1 = 1.540526 \text{ \AA}$ ,  $\lambda_2 = 1.544398 \text{ \AA}$ , 40 kV, 40 mA). The XRD instrument (XRD, D8 Advance, Bruker) was equipped with a high-resolution energy-dispersive 1D detector (LYNXEYE). Mineral samples from anoxic samples were prepared under glovebox atmosphere using oxygen-free ethanol. All XRD scans were collected using an airtight specimen holder (Bruker AXS, A100B138-B141) in Bragg-Brentano geometry from  $10\text{-}70^\circ 2\theta$  in increments of  $0.02^\circ$  and with an acquisition time of 4 s per step. The mineral phase fractions were identified and quantified using Rietveld quantitative phase analysis (QPA)<sup>5</sup> of XRD patterns in TOPAS software (Bruker AXS, Version 5). For the fits, ferrihydrite was included as a mass-calibrated PONKCS<sup>6</sup> phase, as described in previous studies.<sup>7-9</sup> The PONKCS phase was only included in the Rietveld fits if the presence of ferrihydrite was indicated by Fe K-edge EXAFS data (Section S8). Published structure files from the inorganic crystal structure database (ICSD, FIZ Karlsruhe) were used for lepidocrocite (ICSD 93948),<sup>10</sup> goethite (ICSD 239321),<sup>11</sup> magnetite (ICSD 26410),<sup>12</sup> and siderite (ICSD 169789).<sup>13</sup> Crystalline mineral phases were only included in the Rietveld fit if distinct peaks were visible. The preferred orientation of crystals was considered for lepidocrocite (010) and goethite (100, 110) based on the March-Dollase equation implemented in TOPAS.<sup>14</sup>

Mineral fractions in  $^{NA}\text{Fe}$ -mineral samples

**Figure S12:** Iron (Fe) mineral fractions in  $^{NA}\text{Fe}$ -mineral samples from mesh bags without soil for ferrihydrite ( $^{NA}\text{Fe}$ -Fh, A) and lepidocrocite ( $^{NA}\text{Fe}$ -Lp, B) incubated for 12 weeks in the redox fluctuating mesocosms, with Fe-mineral fractions derived from Rietveld analysis of X-ray diffraction patterns, shown as mean values with error bars showing the standard error between experimental triplicates. The Fe-mineral fractions are labeled with Fh = ferrihydrite, Lp = lepidocrocite, Gt = goethite, Mt = magnetite. Siderite fractions were <5% (not labeled, teal area). Selected diffraction patterns and fits are shown in Figure S13, fitting parameters for all fits are presented in Table S3.

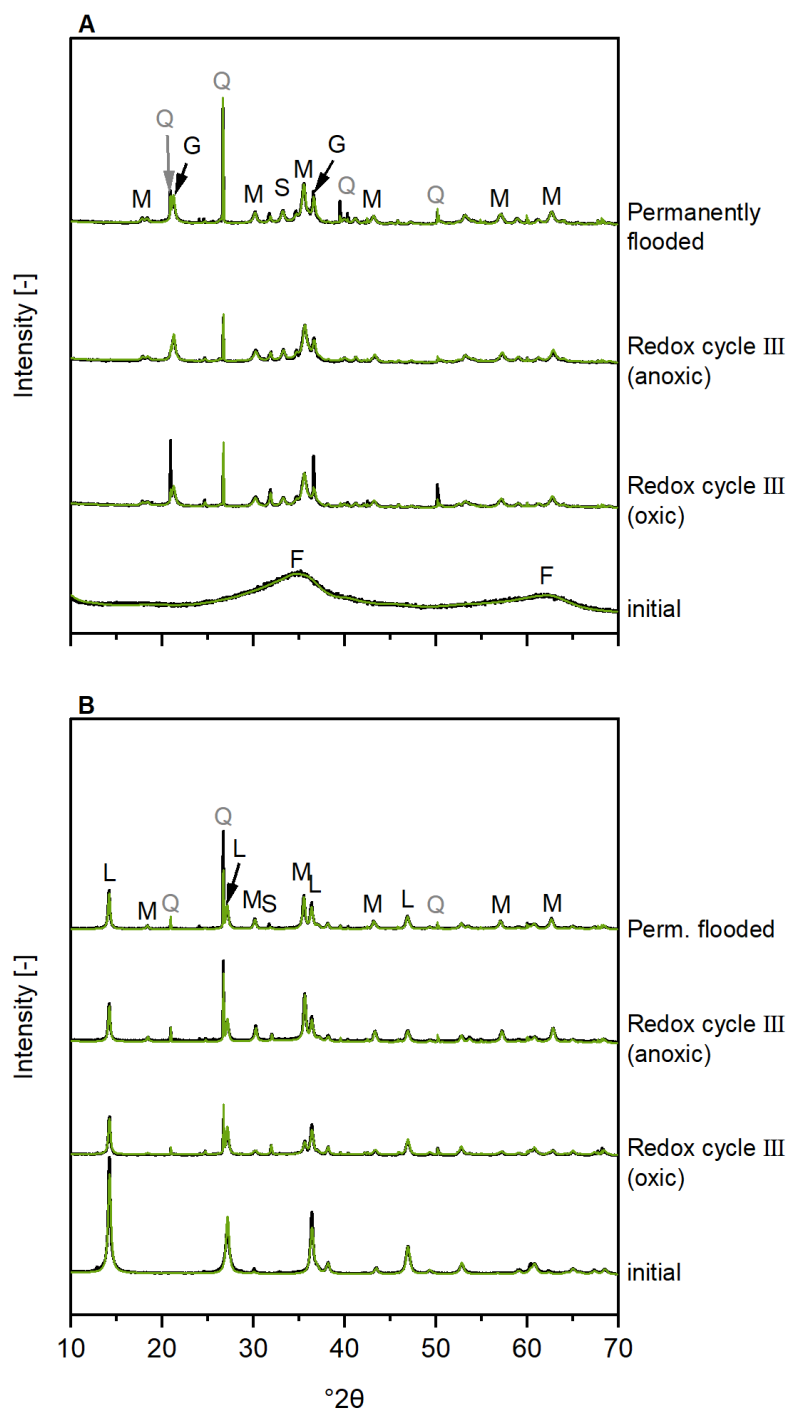


**Figure S13:** X-ray diffraction patterns (black) and corresponding Rietveld fits (green) for  $^{54}\text{Fe}$ -ferrihydrite (A) and  $^{54}\text{Fe}$ -lepidocrocite (B), for initial samples and for samples from redox cycle III (11 and 12 weeks) in the redox fluctuating mesocosms, and from the permanently flooded mesocosm (12 weeks). Main diffraction peaks are labeled with: F = ferrihydrite, L = lepidocrocite, G = goethite, M = magnetite, S = siderite and Q = quartz.

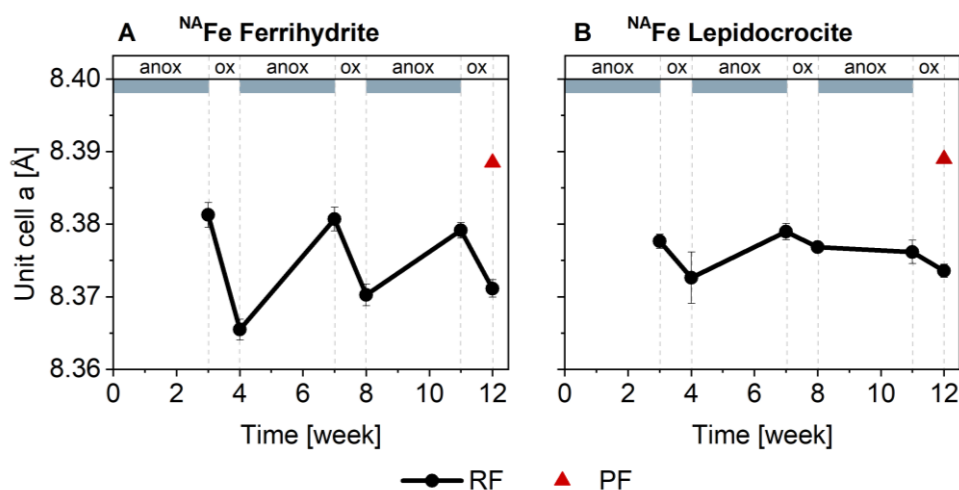
## Fitting parameters

**Table S3:** Fitting parameters and results from Rietveld fits of X-ray diffraction patterns collected from <sup>NA</sup>Fe-mineral samples without soil (<sup>NA</sup>Fe-Fh and <sup>NA</sup>Fe-Lp), reporting the mineral fractions with the standard error between experimental triplicates. The fit quality was similar between the experimental triplicates and the fit evaluation ( $R_{exp}$ ,  $R_{wp}$ , GOF) is therefore reported only for replicate 1 (R1). Abbreviations: w = week, PO = preferred orientation, Lp = lepidocrocite, Gt = goethite, Fh = ferrihydrite, Mt = magnetite, Sd = siderite, se = standard error,  $R_{exp}$  = expected R-factor,  $R_{wp}$  = weighted profile R-factor, GOF = goodness of fit ( $GOF = R_{wp}/R_{exp}$ ).

Mineral	Time [week]	Sample	PO Lp 010	PO Gt 100	PO Gt 110	Fh [-]	Fh_se [-]	Lp [-]	Lp_se [-]	Gt [-]	Gt_se [-]	Mt [-]	Mt_se [-]	Sd [-]	Sd_se [-]	$R_{exp}$ (R1)	$R_{wp}$ (R1)	GOF (R1)
<sup>NA</sup> Fe-Fh	0	initial	-	-	-	1	-	0	-	0	-	0.00	-	0	-	2.56	2.65	1.03
	3	RF - anoxic	-	1.13	0.16	0.39	0.05	0.00	-	0.36	0.07	0.20	0.01	0.04	0.02	5.67	14.23	2.51
	4	RF - oxic	-	1.04	0.55	0.44	0.08	0.00	-	0.35	0.11	0.17	0.03	0.04	0.02	4.25	11.44	2.69
	7	RF - anoxic	-	1.11	0.17	0.34	0.06	0.00	-	0.32	0.07	0.30	0.02	0.04	0.02	5.72	12.13	2.12
	8	RF - oxic	-	1.05	0.52	0.38	0.02	0.00	-	0.33	0.04	0.19	0.01	0.04	0.02	4.72	9.45	2
	11	RF - anoxic	-	1.09	0.18	0.38	0.02	0.00	-	0.38	0.03	0.21	0.04	0.03	0.02	5.64	14.94	2.65
	12	RF - oxic	-	1.1	0.29	0.39	0.04	0.00	-	0.31	0.03	0.28	0.02	0.02	0.01	5.22	8.36	1.6
	12	PF - anoxic	-	1.04	0.2	0.33	0.02	0.00	-	0.35	0.04	0.27	0.01	0.04	0.02	5.3	10.42	1.96
<sup>NA</sup> Fe-Lp	0	initial	0.95	-	-	0	-	1	-	0	-	0	-	0	-	4.3	10.71	2.49
	3	RF - anoxic	0.96	-	-	0.36	0.00	0.38	0.04	0.00	-	0.24	0.03	0.01	0.00	5.31	11.75	2.22
	4	RF - oxic	0.94	-	-	0.35	0.01	0.51	0.05	0.00	-	0.11	0.06	0.03	0.01	4.53	10.74	2.37
	7	RF - anoxic	0.96	-	-	0.35	0.00	0.42	0.06	0.00	-	0.20	0.07	0.02	0.02	4.9	13.24	2.7
	8	RF - oxic	0.92	-	-	0.44	0.02	0.40	0.03	0.00	-	0.15	0.07	0.01	0.01	4.85	10.91	2.25
	11	RF - anoxic	0.96	-	-	0	-	0.66	0.11	0.00	-	0.29	0.12	0.04	0.02	5.2	10.46	2.01
	12	RF - oxic	0.98	-	-	0.42	0.03	0.31	0.04	0.00	-	0.25	0.01	0.01	0.01	4.66	9.2	1.97
	12	PF - anoxic	0.96	-	-	0.38	0.00	0.36	0.02	0.00	-	0.24	0.02	0.01	0.00	5.5	12.25	2.23

### Magnetite stoichiometry

Magnetite is a mixed-valence Fe(II)-Fe(III) mineral and exists at various Fe(II):Fe(III) ratios.<sup>15</sup> The unit cell length (parameter  $a$ ) of magnetite, derived from Rietveld analysis of XRD patterns, can give indications for the Fe(II):Fe(III) ratio in magnetite, with smaller unit cell sizes pointing towards lower Fe(II):Fe(III) ratios in magnetite (stoichiometric magnetite:  $a = 8.396\text{--}8.400$  Å, ref 15, maghemite:  $a = 8.34$  Å, refs 15,16). In this experiment, the unit cell length of magnetite in the  $^{54}\text{Fe}$ -Fh samples during anoxic periods was lower (8.381 Å, redox cycle I), compared to stoichiometric magnetite (Figure S14A). Throughout the redox cycles, the Fe(II):Fe(III) ratio in magnetite in  $^{54}\text{Fe}$ -Fh samples alternated between a more reduced state during anoxic periods (higher unit cell length) and a more oxidized state during oxic periods (lower unit cell length). When magnetite was formed from  $^{54}\text{Fe}$ -Lp, the trends in the unit cell lengths were similar but changes were much smaller (Figure S14B). The results of this study suggest that magnetite stoichiometry can be affected by soil redox fluctuations.

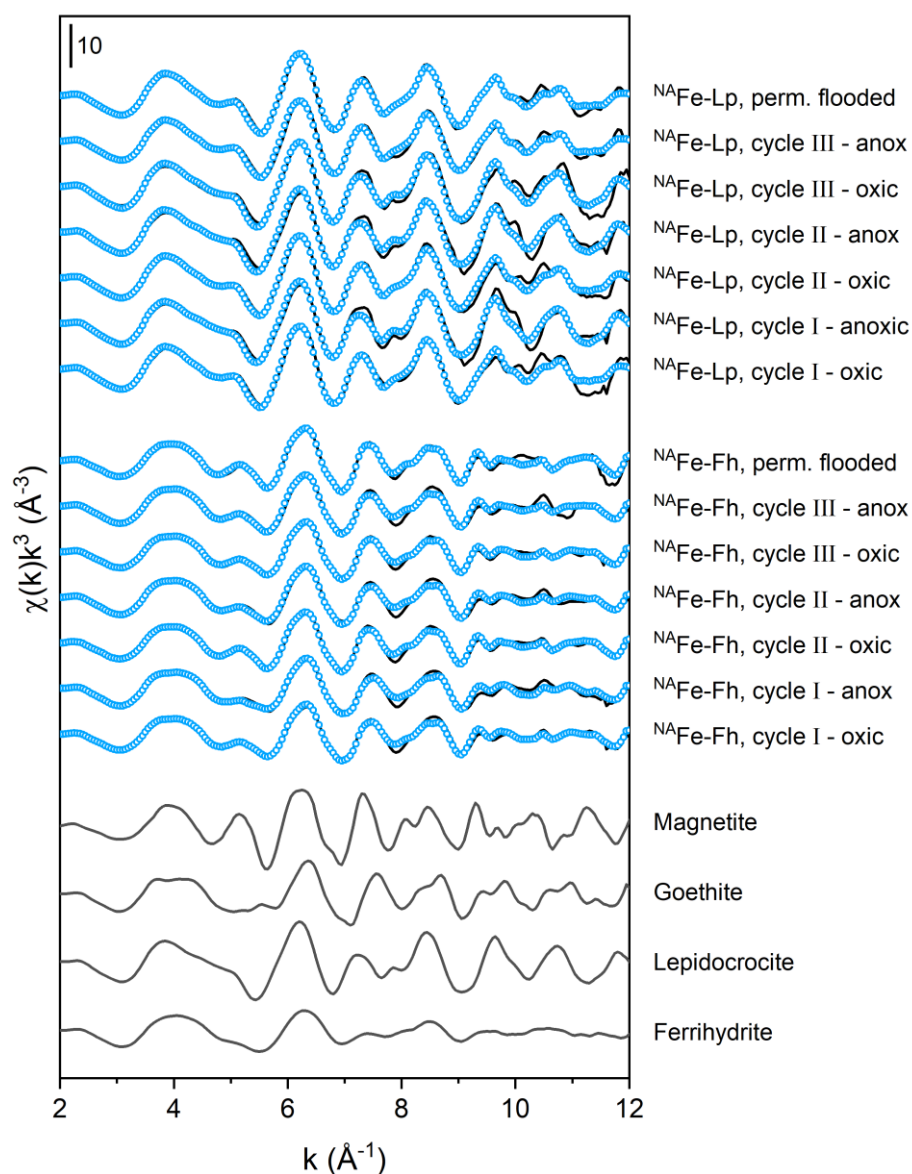


**Figure S14:** Unit cell length (parameter  $a$ ) for magnetite formed in  $^{54}\text{Fe}$ -ferrihydrite (A) and  $^{54}\text{Fe}$ -lepidocrocite (B) mesh bags without soil during the incubation in the redox fluctuating treatment (RF, black line and circles) and the permanently flooded (PF, red triangle) mesocosms for 12 weeks. Labels above grey boxes indicate anoxic (anox, grey boxes) and oxic (ox) periods. Error bars show the standard error between experimental triplicates, errors  $<0.001$  are smaller than symbols and are not shown.

## S8. Fe K-edge X-ray absorption spectroscopy

### Measurement details and fitting

The speciation of solid-phase Fe in  $^{57}\text{Fe}$ -mineral samples was analyzed by bulk Fe K-edge (7112 eV) XAS at the SAMBA beamline of the SOLEIL synchrotron (St. Aubin, France). For these analyses, triplicate samples were combined and pressed into 1.0 cm pellets under  $\text{N}_2$  atmosphere in the glovebox and sealed with Kapton tape. X-ray absorption near edge structure (XANES) and extended X-ray absorption fine structure (EXAFS) spectra were recorded as transmission spectra in continuous measurement mode at  $\sim 80$  K using a  $\text{N}_2$  (l) cryostat. The Si(220) monochromator was calibrated to the first-derivative maximum of the K-edge absorption spectrum of a metallic Fe foil (7112 eV). The foil was continuously monitored to account for small energy shifts ( $<1$  eV) during the sample measurements. Higher harmonics in the beam were eliminated by mirrors. Ten to 16 scans per sample were collected and merged. All spectra were energy calibrated, pre-edge subtracted, and post-edge normalized in Athena<sup>17</sup> with the edge energy,  $E_0$ , defined as the zero-crossing in the second XANES derivative. Linear combination fit (LCF) analyses of  $k^3$ -weighted EXAFS spectra were performed in Athena<sup>17</sup> over a  $k$ -range of 2–12  $\text{\AA}^{-1}$  with the  $E_0$  of all spectra and reference compounds set to 7128 eV. Reference compounds for Fe-minerals were selected based on plausible mineral transformation products of ferrihydrite and lepidocrocite reported in literature<sup>9,18,19</sup> and included ferrihydrite, lepidocrocite, magnetite, goethite, siderite,<sup>20</sup> and green rust carbonate (spectrum courtesy of T. Borch). No constraints were imposed on the fits, and initial fit fractions ( $107 \pm 6\%$ ) were recalculated to a compound sum of 100%. All EXAFS spectra and the corresponding fits are presented in Figure S15, and fit parameters are given in Table S4.

Additional data from Fe K-edge XAS of  $^{54}\text{Fe}$ -mineral samples

**Figure S15:** Fe K-edge EXAFS spectra ( $k$ -weight = 3) of references and linear combination fits of  $^{54}\text{Fe}$ -ferrihydrite ( $^{54}\text{Fe}$ -Fh) and lepidocrocite ( $^{54}\text{Fe}$ -Lp) samples without soil from redox cycles I-III in the redox fluctuating and the permanently (perm.) flooded mesocosms. Experimental data and model fits are shown as solid and dotted lines, respectively. Fit results are presented in Table S4. Abbreviations: anox = anoxic.

**Table S4:** Fit results from linear combination fitting of  $k^3$ -weighted Fe K-edge EXAFS spectra collected from ferrihydrite ( $^{54}\text{Fe}$ -Fh) and lepidocrocite ( $^{54}\text{Fe}$ -Lp) mesh bags without soil. Fitted fractions were corrected to equal a sum of 1. The normalized sum of squared residuals (NSSR) was calculated as  $100 \times \sum_i (\text{data}_i - \text{fit}_i)^2 / \sum_i \text{data}_i^2$ . The fit accuracy is given as reduced (Red.)  $\chi^2$  and was calculated as  $=(N_{\text{idp}}/N_{\text{pts}}) \sum_i ((\text{data}_i - \text{fit}_i)/\epsilon_i)^2 (N_{\text{idp}} - N_{\text{var}})^{-1}$ .  $N_{\text{idp}}$ ,  $N_{\text{pts}}$ , and  $N_{\text{var}}$  are, respectively, the number of independent points in the model fit (20), the total number of data points (201), and the number of fit variables (2-3).  $\epsilon_i$  is the uncertainty of the  $i^{\text{th}}$  data point.<sup>21</sup> Abbreviations: w = week, RF = redox fluctuating mesocosms, PF = permanently flooded mesocosm (shown in gray).

Mineral	Time [week]	Sample	Fh	Lp	Gt	Mt	NSSR [%]	Red. $\chi^2$
$^{54}\text{Fe}$ -Fh	3	RF – anoxic	0.18	-	0.52	0.30	5.09	0.33
	4	RF – oxic	0.33	-	0.51	0.16	8.25	0.59
	7	RF – anoxic	0.17	-	0.44	0.39	3.97	0.28
	8	RF – oxic	0.32	-	0.43	0.25	7.52	0.55
	11	RF – anoxic	0.17	-	0.51	0.32	3.78	0.25
	12	RF – oxic	0.31	-	0.38	0.31	8.87	0.68
	12	PF – anoxic	0.06	-	0.48	0.46	5.66	0.45
	$^{54}\text{Fe}$ -Lp	0	Initial	-	0.84	0.16	-	8.92
3		RF – anoxic	-	0.74	-	0.26	8.34	0.33
4		RF – oxic	-	0.94	-	0.06	8.32	0.59
7		RF – anoxic	-	0.77	-	0.23	5.68	0.28
8		RF – oxic	-	0.92	-	0.08	8.38	0.55
11		RF – anoxic	-	0.89	-	0.11	9.22	0.25
12		RF – oxic	-	0.72	-	0.28	4.43	0.68
12		PF – anoxic	-	0.70	-	0.30	3.31	0.45

### S9. Aqua regia digestion

Part of the  $^{57}\text{Fe}$  escaped from the mesh bags during the incubation, as indicated by a drop in the solid-phase Fe contents (Figure S16A) and a drop in the fractions of  $^{57}\text{Fe}$  ( $f^{57}\text{Fe}$ ) in aqua regia digests (Figure S16B). The Fe likely escaped in the form of aqueous  $^{57}\text{Fe}(\text{II})$  following Fe reductive dissolution of  $^{57}\text{Fe}\text{-Fh}$  and  $^{57}\text{Fe}\text{-Lp}$ , which is supported by slightly elevated  $^{57}\text{Fe}$  fractions ( $f^{57}\text{Fe} = 3\text{-}5\%$ , compared to 2% in  $^{\text{NA}}\text{Fe}$ ) in the soil around the sample holders of  $^{57}\text{Fe}$ -mineral samples (Figure S17). The decrease in  $^{57}\text{Fe}$  isotope fractions in  $^{57}\text{Fe}\text{-Fh}$ -soil mix samples was larger than in  $^{57}\text{Fe}\text{-Lp}$ -soil mix samples, which is in line with the lower stability of ferrihydrite against reductive dissolution compared to lepidocrocite<sup>22</sup> (Figure S16B). The lower  $^{57}\text{Fe}$  content in the samples led to noisier Mössbauer spectra and a higher contribution from soil- $^{57}\text{Fe}$  to the Mössbauer signal (Figure S16C). However, the majority (minimum 71% for  $^{57}\text{Fe}\text{-Fh}$  and minimum 84% for  $^{57}\text{Fe}\text{-Lp}$ -soil mixes) of the Mössbauer signal still came from the initially spiked  $^{57}\text{Fe}$ -minerals after 12 weeks of incubation. In the permanently flooded mesocosm, the escape of  $^{57}\text{Fe}$  was slightly lower, with 87% of the Mössbauer signal coming from the initially spiked  $^{57}\text{Fe}$ -mineral in  $^{57}\text{Fe}\text{-Fh}$  and  $^{57}\text{Fe}\text{-Lp}$ -soil mixes. All Fe contents, isotope fractions and Mössbauer signal fractions are presented in Table S5.

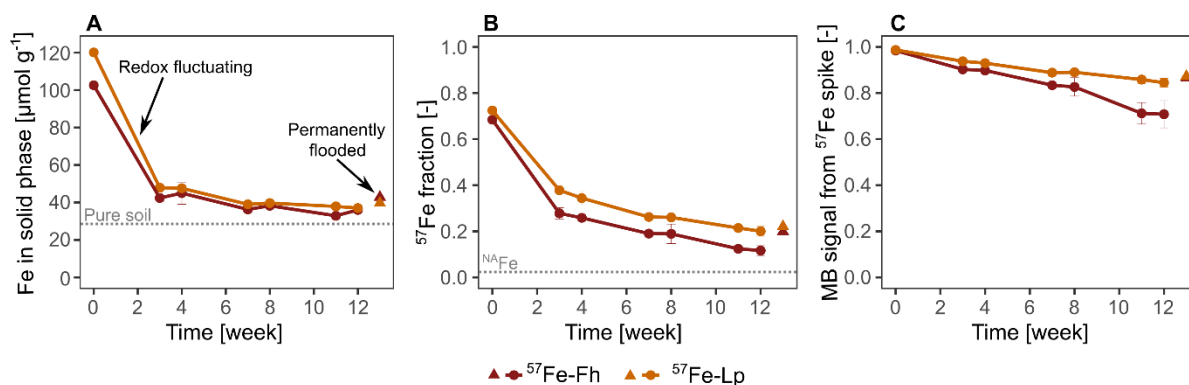


**Figure S16:** Iron (Fe) contents in initial and incubated mineral-soil mixes containing  $^{57}\text{Fe}$ -ferrihydrite ( $^{57}\text{Fe}\text{-Fh}$ ) and  $^{57}\text{Fe}$ -lepidocrocite ( $^{57}\text{Fe}\text{-Lp}$ ) (A), absolute isotope fractions of the  $^{57}\text{Fe}$  isotope in the samples, determined after aqua regia digestion by triple-quadrupole ICP-MS (B), and calculated fractions of the Mössbauer (MB) signal coming from the spiked  $^{57}\text{Fe}$ -labeled minerals (C). Error bars indicate the standard error of experimental triplicates. Errors  $\leq 2 \mu\text{mol g}^{-1}$  in panel A and  $\leq 0.012$  in panels B and C are smaller than symbols and are not shown. Fe contents, Fe isotope fractions and Mössbauer signal fractions from  $^{57}\text{Fe}$ -labeled minerals are presented in Table S5.

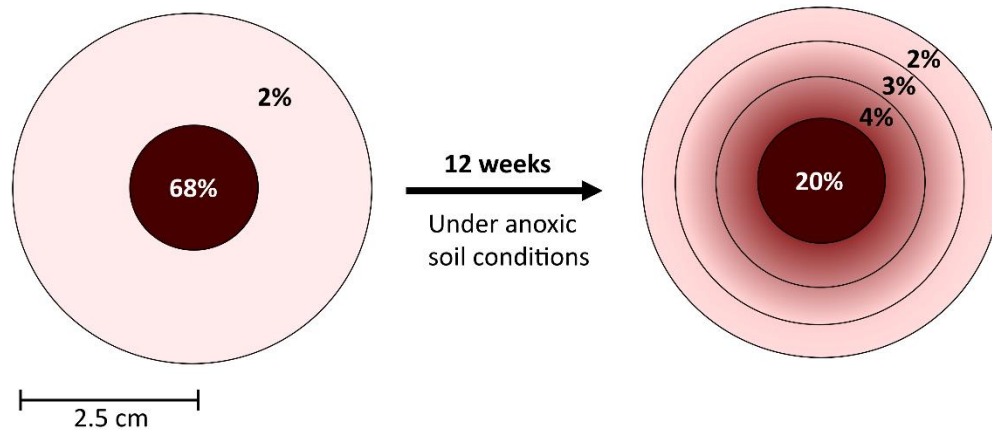


**Figure S17:** Schematic of results from Fe isotope analyses of aqua regia digested  $^{57}\text{Fe}$ -ferrihydrite-soil mixes of inside the mesh bags (small brown circle) and around the sample holders (outer circles) collected with a Humax core sleeve after 12 weeks in the permanently flooded mesocosm. Percentages indicate  $^{57}\text{Fe}$  fractions in the respective samples, relative to the sum (counts per second) of isotope fractions of  $^{54}\text{Fe}$ ,  $^{56}\text{Fe}$ ,  $^{57}\text{Fe}$  and  $^{58}\text{Fe}$ . The corresponding proportions of  $^{57}\text{Fe}$  atoms coming from the added  $^{57}\text{Fe}$ -labeled ferrihydrite in the mineral-soil mixes are 98% and 87% before and after the incubation, respectively. The color gradient is provided for visual aid. All Fe contents and Fe isotope fractions are presented in Table S5.

**Table S5:** Iron (Fe) concentrations in aqua regia digests of initial and incubated samples from mineral-soil mixes containing  $^{57}\text{Fe}$ -ferrihydrite ( $^{57}\text{Fe}$ -Fh) or  $^{57}\text{Fe}$ -lepidocrocite ( $^{57}\text{Fe}$ -Lp), isotope fractions of  $^{54}\text{Fe}$  ( $f^{54}\text{Fe}$ ),  $^{56}\text{Fe}$  ( $f^{56}\text{Fe}$ ),  $^{57}\text{Fe}$  ( $f^{57}\text{Fe}$ ) and  $^{58}\text{Fe}$  ( $f^{58}\text{Fe}$ ), and the corresponding fraction of the Mössbauer signal (Frac. MB signal) coming from the initially spiked  $^{57}\text{Fe}$ . Standard errors (se) were calculated from the results from experimental triplicates. Abbreviation: PF = permanently flooded mesocosm.

Time	Fe	se	$f^{54}\text{Fe}$	se	$f^{56}\text{Fe}$	se	$f^{57}\text{Fe}$	se	$f^{58}\text{Fe}$	se	Frac. MB signal	se
week	$\mu\text{mol g}^{-1}$		-								-	
<b><math>^{57}\text{Fe}</math>-Fh-soil mix</b>												
0	102.55	-	0.02	-	0.28	-	0.68	-	0.02	-	0.98	-
3	42.40	1.66	0.04	0.00	0.67	0.02	0.28	0.02	0.01	0.00	0.90	0.01
4	44.99	5.87	0.04	0.00	0.69	0.02	0.26	0.02	0.01	0.00	0.90	0.02
7	36.29	0.84	0.05	0.00	0.76	0.02	0.19	0.02	0.01	0.00	0.83	0.02
8	38.24	1.74	0.05	0.00	0.76	0.04	0.19	0.04	0.01	0.00	0.83	0.04
11	32.90	1.86	0.05	0.00	0.82	0.02	0.12	0.02	0.01	0.00	0.71	0.05
12	36.01	2.07	0.05	0.00	0.83	0.02	0.12	0.02	0.00	0.00	0.71	0.06
12_PF	42.85	4.22	0.04	0.00	0.75	0.01	0.20	0.01	0.01	0.00	0.87	0.0084
<b>Humax core around <math>^{57}\text{Fe}</math>-Fh-soil mix</b>												
12_PF	29.34	-	0.05	-	0.90	-	0.04	-	0.00	-	-	-
12_PF	31.55	-	0.06	-	0.92	-	0.03	-	0.00	-	-	-
12_PF	30.73	-	0.06	-	0.92	-	0.02	-	0.00	-	-	-

Table S5: continued.

Time	Fe	se	$f^{54}\text{Fe}$	se	$f^{56}\text{Fe}$	se	$f^{57}\text{Fe}$	se	$f^{58}\text{Fe}$	se	Frac. MB signal	se
week	$\mu\text{mol g}^{-1}$											
-												
<b><math>^{57}\text{Fe-Lp-soil mix}</math></b>												
0	120.07	-	0.01	-	0.24	-	0.72	-	0.02	-	0.99	-
3	47.86	1.68	0.03	0.00	0.58	0.01	0.38	0.01	0.01	0.00	0.94	0.00
4	47.58	2.28	0.04	0.00	0.61	0.03	0.34	0.03	0.01	0.00	0.93	0.01
7	39.00	1.73	0.04	0.00	0.69	0.02	0.26	0.02	0.01	0.00	0.89	0.01
8	39.67	1.44	0.04	0.00	0.69	0.02	0.26	0.02	0.01	0.00	0.89	0.01
11	37.89	1.85	0.04	0.00	0.73	0.02	0.21	0.02	0.01	0.00	0.86	0.02
12	37.00	1.06	0.05	0.00	0.75	0.02	0.20	0.02	0.01	0.00	0.84	0.02
12_PF	37.71	0.76	0.04	0.00	0.73	0.00	0.22	0.00	0.01	0.00	0.87	0.0032
<b>Humax core around <math>^{57}\text{Fe-Lp-soil mix}</math></b>												
12_PF	28.05	-	0.05	-	0.90	-	0.05	-	0.00	-	-	-
12_PF	29.39	-	0.05	-	0.90	-	0.04	-	0.00	-	-	-
12_PF	27.86	-	0.05	-	0.91	-	0.03	-	0.00	-	-	-

**S10. Sequential iron extractions**

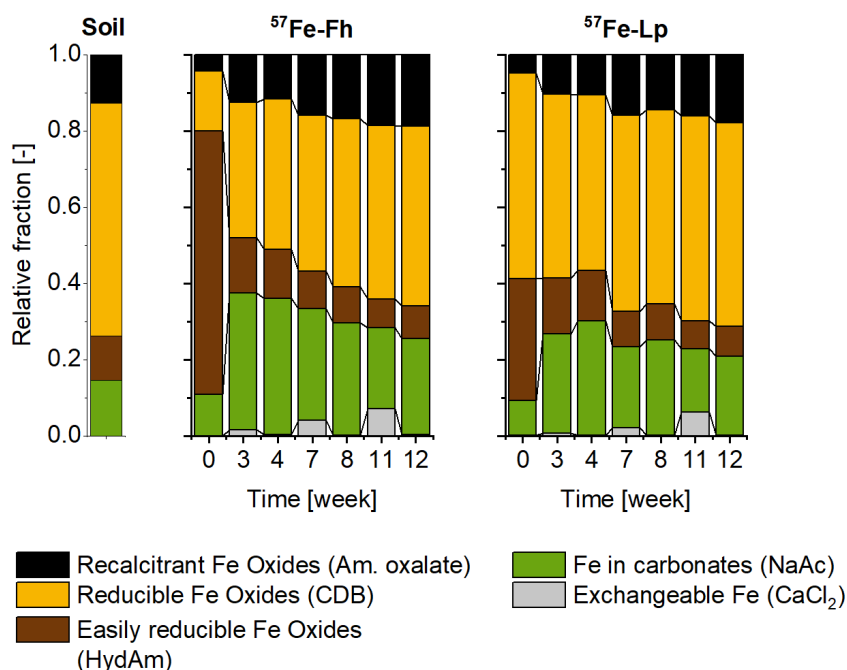
The reactive Fe fractions in mineral-soil mixes was assessed by a five-step Fe sequential extraction, following the method of Poulton and Canfield.<sup>3</sup> Approximately 100-150 mg of the dried mineral-soil mixes were weighed into 15 mL centrifuge tubes in the glovebox, and the exact weight was recorded. All extraction steps are summarized in Table S6. Steps 1-3 were conducted in the glovebox, and steps 4 and 5 were performed under N<sub>2</sub> flow outside the glovebox. In each step, 10 mL of the respective extraction solution was added to the solid samples, shaken on an overhead shaker for the respective extraction period, and centrifuged at 3800 g for 15 min before the solution was decanted and filtered through a 0.22 µm nylon filter. The Fe concentration in the extractants was analyzed by ICP-OES, including internal quality controls with the respective matrix of the extraction solution.

**Table S6:** Sequential iron extraction steps

Step	Extraction step	Time [h]	Targeting	Reference
1	1 M CaCl <sub>2</sub> , pH 7	2	Exchangeable Fe	3
2	1 M Na-acetate, buffered to pH 4.5 with acetic acid	24	Fe in carbonates, e.g., siderite	3
3	1 M hydroxylamine-HCl with 25 vol-% acetic acid	24	Easily reducible, amorphous Fe oxides, e.g., ferrihydrite	3 and 23
4	Citrate dithionite bicarbonate (CDB) containing 0.35 M glacial acetic acid, 0.2 M Na citrate with 50 g L <sup>-1</sup> Na dithionite at pH 4.8	2	Reducible Fe oxides, e.g., goethite, hematite	3
5	0.2 M ammonium oxalate, 0.17 M oxalic acid at pH 3.2	6	Recalcitrant Fe oxides, e.g. magnetite	3

Ferrihydrite in initial <sup>57</sup>Fe-Fh-soil mixes was most likely extracted with the fraction of easily reducible Fe oxides,<sup>3</sup> as indicated by the larger hydroxylamine-HCl fraction in <sup>57</sup>Fe-Fh-soil mixes compared to the soil without added mineral (Section S1). For the <sup>57</sup>Fe-Lp-soil mixes, part of the lepidocrocite was likely extracted in the fraction of easily reducible Fe oxides.<sup>3</sup> Remaining lepidocrocite likely was extracted with the fraction of reducible Fe oxides,<sup>3</sup> as suggested by the increased citrate-dithionite-bicarbonate fraction in <sup>57</sup>Fe-Lp-soil mixes compared to the soil without added mineral (Section S1). The results for the incubated <sup>57</sup>Fe-Fh- and <sup>57</sup>Fe-Lp-soil mixes show that the biggest changes occurred in the fraction of easily reducible Fe oxides and the fraction of Fe in carbonates, compared to the initial mineral-soil mixes (Figure S18). The decreased fraction of easily reducible Fe oxides (including ferrihydrite and lepidocrocite, ref 3) in incubated samples compared to the initial mineral-soil mixes indicates that ferrihydrite and lepidocrocite were reductively dissolved in the <sup>57</sup>Fe-Fh- and <sup>57</sup>Fe-Lp-soil mixes, respectively (Figure S18). In turn, the Fe fraction extracted by sodium acetate (NaAc) increased upon the start of the incubation of the <sup>57</sup>Fe-Fh- and <sup>57</sup>Fe-Lp-soil mixes. This extraction step targets Fe in carbonates. Still, we expect that this step also extracted part of the highly disordered mixed-valence Fe phase, which was observed as a collapsed feature in the Mössbauer spectra (5 K) and is discussed in more detail in Section S11. Further, the fraction extracted by CaCl<sub>2</sub> indicated that adsorbed Fe was

present, especially in samples from anoxic periods (Figure S18). The adsorbed Fe fraction most likely consisted of Fe(II). This is supported by Mössbauer results, which showed adsorbed Fe(II) in all mineral-soil mix samples (Figure 4). Due to the escape of  $^{57}\text{Fe}$  from the mesh bags, as indicated by aqua regia results (Figure S16 and Figure S17), we expect a slight relative increase in the fraction of reducible Fe oxides (CDB) throughout the incubation due to increased contributions from the soil, where the CDB fraction was most prominent (Figure S2).

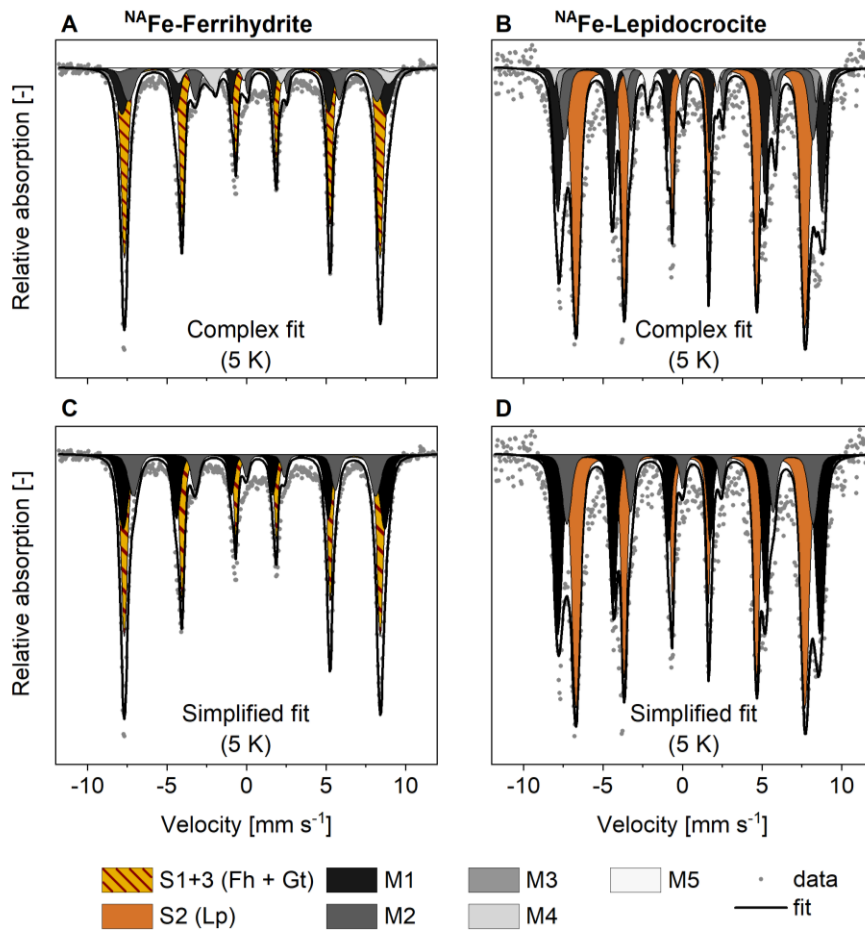


**Figure S18:** Sequential iron (Fe) extraction results from  $^{57}\text{Fe}$ -ferrihydrite ( $^{57}\text{Fe}$ -Fh) and  $^{57}\text{Fe}$ -lepidocrocite ( $^{57}\text{Fe}$ -Lp) soil mixes for the pure soil and the initial (0 weeks) and reacted samples collected after the anoxic (3, 7 and 11 weeks) and the oxic (4, 8 and 12 weeks) periods.

## **S11. Mössbauer spectroscopy**

### **Sample preparation and measurement details**

For  $^{57}\text{Fe}$ -mineral-soil mix samples, triplicate samples were combined and an aliquot of ~150 mg was sealed in two layers of Kapton tape (diameter of sample ~1 cm). For pure  $^{NA}\text{Fe}$ -mineral samples, triplicate samples were combined and ~15 mg of the mineral was suspended in 1.5 mL ultra-pure water, deposited onto a 0.22  $\mu\text{m}$  PVDF filter using a syringe and air-dried in the dark in the glovebox (anoxic samples) or in ambient air (oxic samples), before the samples were sealed in two layers of Kapton tape. The spectrometer was equipped with a  $^{57}\text{Co}$  source in a standard setup (WissEl, Wissenschaftliche Elektronik GmbH) and a closed-cycle cryostat (SHI-850, Janis Research Co.). A 7  $\mu\text{m}$  thick  $\alpha\text{-Fe(0)}$  foil was used for calibration at room temperature. The spectra were fitted using the Recoil software<sup>24</sup> by applying an extended Voigt-based fitting routine, with the half-width at half-maximum fixed to 0.135  $\text{mm s}^{-1}$ , which is the inner line broadening of the calibration foil.

Magnetite fitting in  $^{54}\text{Fe}$ -mineral samples (permanently flooded mesocosm)

**Figure S19:** Mössbauer spectra of  $^{54}\text{Fe}$ -ferrihydrate and  $^{54}\text{Fe}$ -lepidocrocite samples after the incubation in the permanently flooded mesocosm for 12 weeks, adopting the fitting approach for magnetite suggested by Doriguetto et al.<sup>25</sup> with five magnetite sextets (M1-M5; A, B) or using a simplified fitting approach with two magnetite sextets (M1 and M2; C, D). Magnetite sextets M1 and M2 correspond to sextets S4 and S5 in the main text. Sextet S1+3 was interpreted as a mixture of goethite (Gt) and ferrihydrate (Fh), sextet S2 was interpreted as lepidocrocite (Lp).

Additional data (77 K and 295 K)

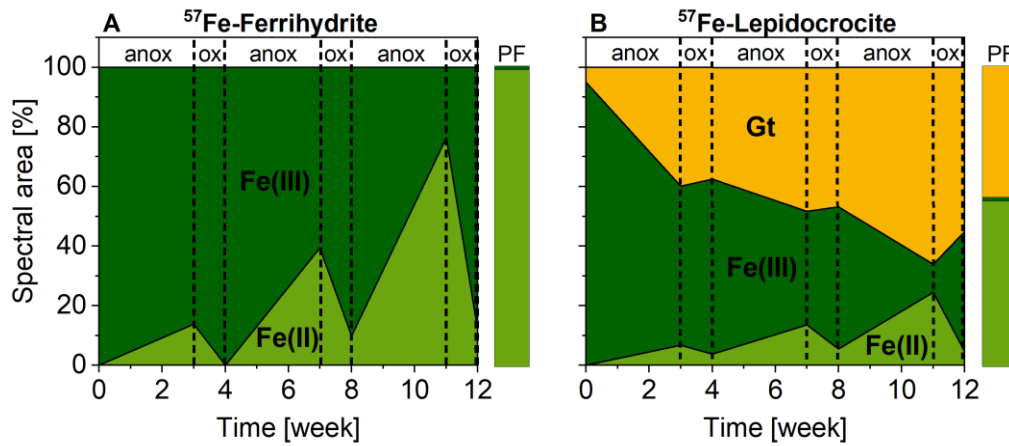


**Figure S20:** Fitted fractions of Fe(II), Fe(III) and goethite (Gt) in 77 K Mössbauer spectra of  $^{57}\text{Fe}$ -ferrihydrate- (A) and  $^{57}\text{Fe}$ -lepidocrocite- (B) soil mixes incubated in the redox fluctuating mesocosms (area graphs) with anoxic (anox) and oxic (ox) periods, and in the permanently flooded mesocosm after 12 weeks (PF, bar graphs).

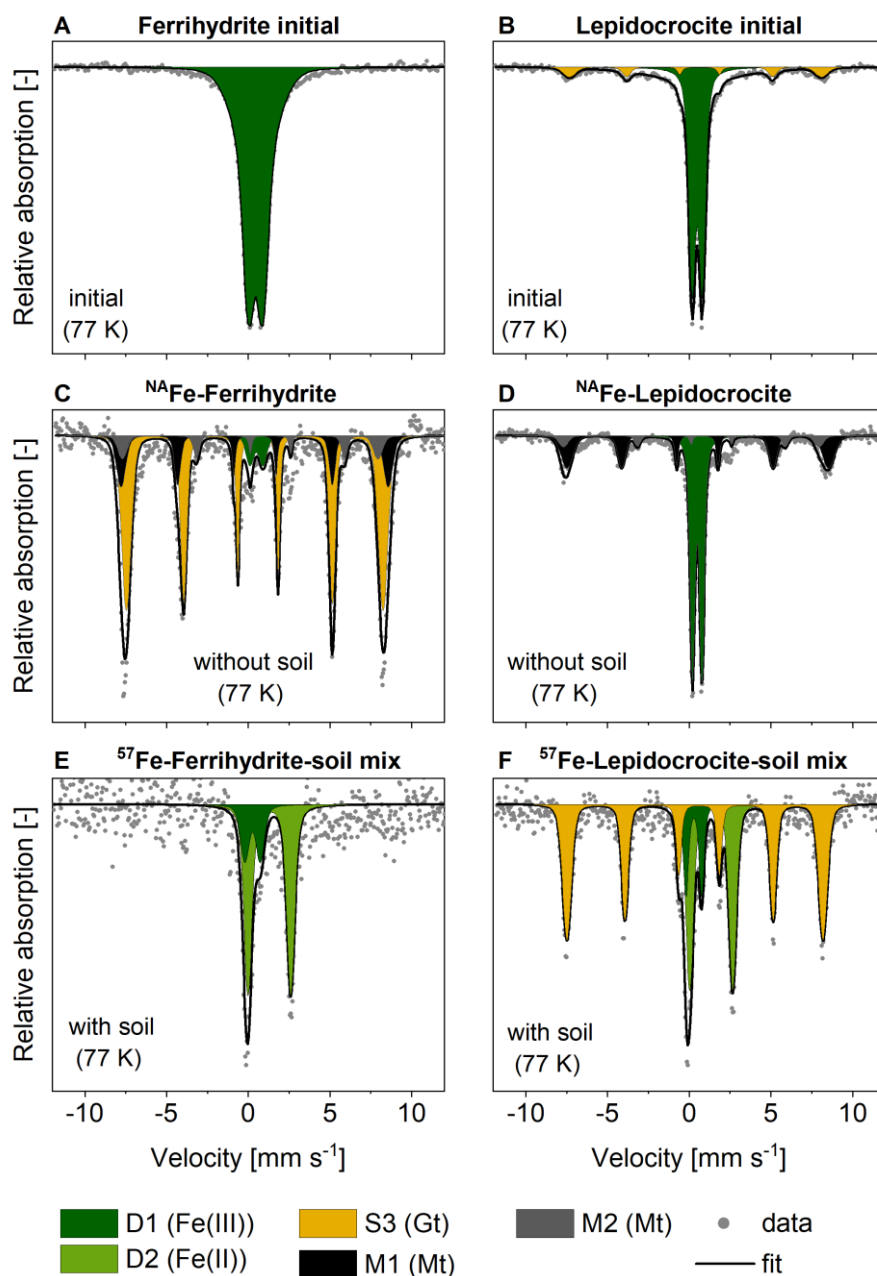


**Figure S21:** Mössbauer spectra (77 K) of initial <sup>57</sup>Fe-ferrihydrate (A) and <sup>57</sup>Fe-lepidocrocite-soil mixes (B) and 11-week samples incubated in the redox fluctuating mesocosms (C-D), with ferrihydrate incubated as <sup>NA</sup>Fe-mineral mesh bags without soil (C, D) or <sup>57</sup>Fe-mineral-soil mixes (E, F). Fitting parameters for magnetite sextets (M1, M2) were derived from Doriguetto et al.<sup>25</sup> Abbreviations: Gt = goethite, Mt = magnetite.

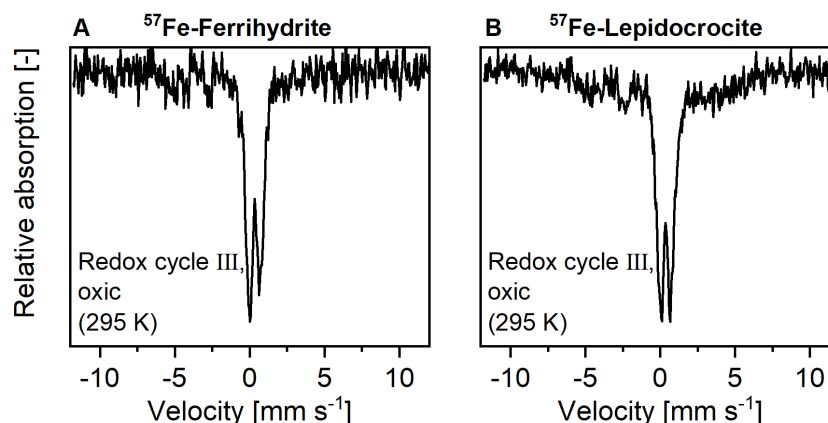


**Figure S22:** Room temperature (295 K) Mössbauer spectra of  $^{57}\text{Fe}$ -mineral-soil mixes incubated in the redox fluctuating mesocosms for 12 weeks (redox cycle III, oxic period), confirming the absence of magnetite in these samples, which would form a sextet at room temperature.

#### **Collapsed feature in Mössbauer spectra**

A collapsed feature was required for fitting the Mössbauer spectra of incubated  $^{57}\text{Fe}$ -Fh and  $^{57}\text{Fe}$ -Lp samples, indicating the presence of a  $^{57}\text{Fe}$  phase with a magnetic ordering temperature close to 5 K. This phase was, therefore, not fully magnetically ordered at 5 K, and fitting parameters were not specific enough to identify the Fe phase. Previous studies have assigned similar features to a highly disordered Fe phase which was likely coprecipitated with organic matter and/or other dissolved soil components.<sup>1,26,27</sup> The formation of a mixed-valence disordered Fe phase is additionally supported by the results from the Fe sequential extractions, where the fraction of Fe extracted in the sodium acetate step increased with the incubation of the mineral-soil mixes (Figure S18). The sodium acetate step is supposed to target Fe carbonates.<sup>3</sup> However, labile short range-ordered Fe phases may be extracted as well, since the Fe extraction with sodium acetate works through a drop in pH (to 4.5). Further, the comparison between the 77 K and the 5 K spectra showed much higher Fe(II) fractions in the spectra collected at 77 K, than at 5 K (e.g. for the 11-week  $^{57}\text{Fe}$ -Fh-soil mix sample 76% at 77 K versus 46% at 5 K, Figure S23). This suggests that the collapsed feature contains a mixed-valence Fe phase, with large fractions of Fe(II).

The Fe(II) in the mixed-valence disordered Fe phase could either be Fe(II) which was stabilized against oxidation by organic matter,<sup>28</sup> or it could be part of Fe(II)-mineral phases, such as vivianite or siderite, which have their magnetic ordering temperature (Néel temperature) between 77 K and 5 K.<sup>29,30</sup> Therefore, it is possible that small amounts of siderite or vivianite were present. Alternatively, the Fe(II) could be part of a green rust-like phase, as observed by Notini et al.<sup>31</sup> Attempts to use a similar fitting approach for our 5 K Mössbauer spectra, using the parameters reported for the green rust-like feature,<sup>31</sup> did not result in satisfactory fits, suggesting that green rust is not a major Fe phase in these samples. Therefore, we interpret the Fe(II) in the mixed-valence disordered Fe phase as Fe(II) stabilized by organic matter or other dissolved soil components, which may contain small fractions of siderite, vivianite, or green rust.

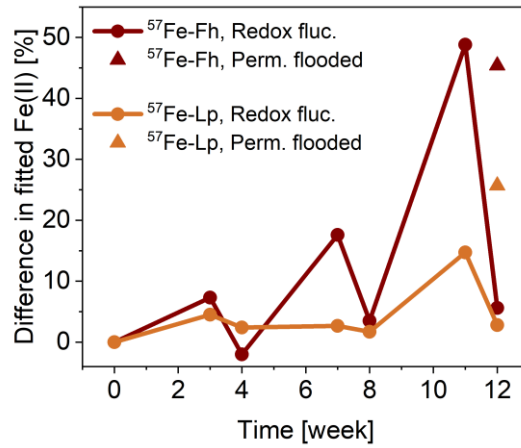


**Figure S23:** Difference in fitted Fe(II) fractions in Mössbauer spectra from <sup>57</sup>Fe-ferrhydrite- (<sup>57</sup>Fe-Fh) and <sup>57</sup>Fe lepidocrocite (<sup>57</sup>Fe-Lp) -soil mixes, collected at 77 K, compared to spectra collected at 5 K (calculated as Fe(II) fraction at 77 K subtracted from Fe(II) fraction at 5 K), suggesting that part of the Fe(II) in the incubated <sup>57</sup>Fe-mineral-soil mixes was part of an Fe phase that starts to order magnetically at 5 K.

Fitting parameters (77 K) of  $^{57}\text{Fe}$ -mineral-soil mixes**Table S7:** Mössbauer fitting parameters for spectra collected from incubated  $^{57}\text{Fe}$ -ferrihydrite-soil mixes ( $^{57}\text{Fe}$ -Fh) at 77 K.

Sample	Time [week]	Type	Component	CS <sup>a</sup> [mm s <sup>-1</sup> ]	QS <sup>b</sup> [mm s <sup>-1</sup> ]	$\sigma_{\text{QS}}$ <sup>c</sup> [mm s <sup>-1</sup> ]	Area [%]	Red. $\chi^2$ <sup>d</sup>
$^{57}\text{Fe}$ -Fh (77 K)	3	RF – anoxic	D1 – Fe(III)	0.46	0.86	0.39	87.6	0.60
			D2 – Fe(II)	1.20*	2.63	0.60	12.4	
	4	RF – oxic	D1 – Fe(III)	0.47	0.81	0.35	100.0	0.69
			D2 – Fe(II)	-	-	-	0.0	
	7	RF – anoxic	D1 – Fe(III)	0.47	0.87	0.45	60.6	0.61
			D2 – Fe(II)	1.27	2.71	0.22	39.4	
	8	RF – oxic	D1 – Fe(III)	0.48	0.80	0.38	92.0	0.87
			D2 – Fe(II)	1.20*	2.70*	0.50*	8.0	
	11	RF – anoxic	D1 – Fe(III)	0.47*	0.80*	0.40*	24.5	0.67
			D2 – Fe(II)	1.29	2.62	0.36	75.5	
	12	RF – oxic	D1 – Fe(III)	0.47	0.81	0.36	88.1	0.96
			D2 – Fe(II)	1.20*	2.70*	0.50*	11.9	
	12	PF – anoxic	D1 – Fe(III)	0.47*	0.80*	0.40*	19.8	0.91
			D2 – Fe(II)	1.29	2.63	0.35	81.2	

<sup>a</sup> CS, Center shift;<sup>b</sup> QS, Quadrupole splitting (for doublets);<sup>c</sup>  $\sigma$ , standard deviation of QS,  $\epsilon$  or H;<sup>d</sup> Reduced  $\chi^2$ , goodness of fit;

\* Indicates values that were fixed during the fitting process.

Abbreviations: RF = redox fluctuating mesocosms, PF = permanently flooded mesocosm, D = doublet, S = sextet.

**Table S8:** Mössbauer fitting parameters for spectra collected from incubated <sup>57</sup>Fe lepidocrocite-soil mixes (<sup>57</sup>Fe-Lp) at 77 K.

Sample	Time [week]	Type	Component	CS <sup>a</sup> [mm s <sup>-1</sup> ]	QS <sup>b</sup> or ε <sup>c</sup> [mm s <sup>-1</sup> ]	σ <sub>QS</sub> or σ <sub>ε</sub> <sup>d</sup> [mm s <sup>-1</sup> ]	H <sup>e</sup> [T]	σ <sub>H</sub> <sup>d</sup> [T]	Area [%]	Red. χ <sup>2f</sup>
<sup>57</sup> Fe-Lp (77 K)	3	RF – anoxic	D1 – Fe(III)	0.49	0.77	0.37	-	-	52.2	1.04
			D2 – Fe(II)	1.20*	3.11	0.40*	-	-	7.0	
			S3 – Gt	0.48	-0.10	0.17	47.52	3.22	40.8	
	4	RF – oxic	D1 – Fe(III)	0.48	0.80	0.36	-	-	58.2	1.11
			D2 – Fe(II)	1.20*	3.12	0.40*	-	-	3.7	
			S3 – Gt	0.48	-0.12	-	48.32	2.11	38.1	
	7	RF – anoxic	D1 – Fe(III)	0.48	0.85	0.37	-	-	38.1	0.58
			D2 – Fe(II)	1.20	2.74	0.40	-	-	13.6	
			S3 – Gt	0.44	-0.12	-	48.50	1.64	48.2	
8	RF – oxic	D1 – Fe(III)	0.47	0.81	0.35	-	-	49.2	0.57	
		D2 – Fe(II)	1.20*	3.33	0.40*	-	-	3.3		
		S3 – Gt	0.47	-0.14	-	48.54	1.38	47.5		
11	RF – anoxic	D1 – Fe(III)	0.47*	0.80*	0.50*	-	-	13.9	0.76	
		D2 – Fe(II)	1.29	2.75	0.34	-	-	32.0		
		S3 – Gt	0.48	-0.13	-	48.64	1.46	54.1		
12	RF – oxic	D1 – Fe(III)	0.46	0.82	0.36	-	-	40.2	0.57	
		D2 – Fe(II)	1.21	2.23	0.75	-	-	4.6		
		S3 – Gt	0.46	-0.12	-	48.29	1.16	55.2		
12	PF – anoxic	D1 – Fe(III)	0.47*	0.80*	0.5*	-	-	15.4	0.73	
		D2 – Fe(II)	1.28	2.73	0.31	-	-	47.2		
		S3 – Gt	0.49	-0.11	-	48.78	1.41	37.4		

<sup>a</sup> CS, Center shift;<sup>b</sup> QS, Quadrupole splitting (for doublets);<sup>c</sup> ε, Quadrupole shift (for sextets);<sup>d</sup> σ, standard deviation of QS, ε or H;<sup>e</sup> H, Hyperfine field;<sup>f</sup> Reduced χ<sup>2</sup>, goodness of fit;

\* Indicates values that were fixed during the fitting process.

Abbreviations: RF = redox fluctuating mesocosms, PF = permanently flooded mesocosm, D = doublet, S = sextet, Gt = goethite.

Fitting parameters (5 K) of  $^{57}\text{Fe}$ -mineral-soil mixes**Table S9:** Mössbauer fitting parameters for spectra collected from incubated  $^{57}\text{Fe}$ -ferrihydrite-soil mixes ( $^{57}\text{Fe}$ -Fh) at 5 K. The values corresponding to the use of multiple components (H1, H2) for parameters are marked in brown and were used for fitting lepidocrocite (S2 – Lp).

Sample	Time [week]	Type	Component	CS <sup>a</sup> [mm s <sup>-1</sup> ]	QS <sup>b</sup> or $\varepsilon$ <sup>c</sup> [mm s <sup>-1</sup> ]	$\sigma_{\text{QS}}$ or $\sigma_{\varepsilon}$ <sup>d</sup> [mm s <sup>-1</sup> ]	H <sup>e</sup> [T]	$\sigma_{\text{H}}$ <sup>d</sup> [T]	Area [%]	Red. $\chi^2$ <sup>f</sup>			
$^{57}\text{Fe}$ -Fh (5 K)	3	RF – anoxic	D1 – Fe(III)	0.47	0.97	0.46	-	-	7.9	0.64			
			D2 – Fe(II)	1.21	0.63	0.21	-	-	5.1				
			S1 – Fh	0.47*	-0.01*	0.19*	48.84*	2.74*	36.5				
			S2 – Lp	0.48	0.005*	-	42.86	2.98	24.2				
			H1				45.0*	1.5*					
			H2				42.0*	3.0*					
			Frac. H2					71%					
			CF	0.50*	0.00*	-	26.01*	18.67*	26.3				
			4	RF – oxic	D1 – Fe(III)	0.49	0.82	0.39	-		-	8.5	0.78
					D2 – Fe(II)	1.20*	2.64	0.50*	-		-	2.0	
S1 – Fh	0.47*	-0.01*			0.19*	48.84*	2.74*	38.5					
S2 – Lp	0.50	0.005*			-	43.05	2.94	32.2					
H1						45.0*	1.5*						
H2						42.0*	3.0*						
Frac. H2							65%						
CF	0.50*	0.00*			-	26.01*	18.67*	18.8					
7	RF – anoxic	D1 – Fe(III)			0.46	0.85	0.40	-	-	13.9	0.72		
		D2 – Fe(II)			1.16	3.02	0.93	-	-	21.8			
		S1 – Fh	0.47*	-0.01*	0.19*	48.84*	2.74*	23.5					
		S2 – Lp	0.47	0.005*	-	42.00*	3.00*	5.9					
		CF	1.00*	0.00*	-	26.01*	18.67*	34.8					

Table S9: continued.

Sample	Time [week]	Type	Component	CS <sup>a</sup> [mm s <sup>-1</sup> ]	QS <sup>b</sup> or $\epsilon$ <sup>c</sup> [mm s <sup>-1</sup> ]	$\sigma_{QS}$ or $\sigma_{\epsilon}$ <sup>d</sup> [mm s <sup>-1</sup> ]	H <sup>e</sup> [T]	$\sigma_H$ <sup>d</sup> [T]	Area [%]	Red. $\chi^2$ <sup>f</sup>
<sup>57</sup> Fe-Fh (5 K)	8	RF – oxic	D1 – Fe(III)	0.45	0.79	0.40	-	-	15.7	0.65
			D2 – Fe(II)	1.12	2.73	0.68	-	-	4.5	
			S1 – Fh	0.47*	-0.01*	0.19*	48.84*	2.74*	38.2	
			S2 – Lp	0.49	0.02	-	42.78	3.00	29	
			H1				45.0*	1.5*		
			H2				42.0*	3.0*		
			Frac. H2					74%		
11	RF – anoxic	D1 – Fe(III)	0.48*	0.80*	0.40*	-	-	3.4	0.70	
		D2 – Fe(II)	1.26	2.83	0.63	-	-	28.0		
		S1 – Fh	0.47*	-0.01*	0.19*	48.84*	2.74*	22.7		
		S2 – Lp	-	-	-	-	-	0.0		
		CF	1.00*	0.00*	-	26.01*	18.67*	45.8		
12	RF – oxic	D1 – Fe(III)	0.48*	0.73	0.20	-	-	21.8	0.76	
		D2 – Fe(II)	1.20	2.70	0.50	-	-	6.3		
		S1 – Fh	0.47*	-0.01*	0.19*	48.84*	2.74*	35.2		
		S2 – Lp	0.49	0.005	-	42.66	3.01	25.8		
		H1				45.0*	1.5*			
H2				42.0*	3.0*					
Frac. H2					78%					
12	PF – anoxic	D1 – Fe(III)	0.48*	0.80*	0.40*	-	-	6.5	1.13	
		D2 – Fe(II)	1.23	3.02	0.82	-	-	35.8		
		S1 – Fh	0.47*	-0.01*	0.19*	48.84*	2.74*	9.8		
		S2 – Lp	-	-	-	-	-	0		
		CF	1.00*	0.00*	-	26.01*	18.67*	47.9		

<sup>a</sup> CS, Center shift;<sup>c</sup>  $\epsilon$ , Quadrupole shift (for sextets);<sup>e</sup> H, Hyperfine field;<sup>b</sup> QS, Quadrupole splitting (for doublets);<sup>d</sup>  $\sigma$ , standard deviation of QS,  $\epsilon$  or H;<sup>f</sup> Reduced  $\chi^2$ , goodness of fit;

\* Indicates values that were fixed during the fitting process.

Abbreviations: RF = redox fluctuating mesocosms, PF = permanently flooded mesocosm, D = doublet, S = sextet, Fh = ferrihydrite, Lp = lepidocrocite, CF = collapsed feature.

**Table S10:** Mössbauer fitting parameters for spectra collected from incubated  $^{57}\text{Fe}$ -lepidocrocite-soil mixes ( $^{57}\text{Fe}$ -Lp) at 5 K. Values corresponding to the use of multiple components (H1, H2) for parameters are marked in brown and were used for lepidocrocite (S2 – Lp).

Sample	Time [week]	Type	Component	CS <sup>a</sup> [mm s <sup>-1</sup> ]	QS <sup>b</sup> or $\varepsilon$ <sup>c</sup> [mm s <sup>-1</sup> ]	$\sigma_{\text{QS}}$ or $\sigma_{\varepsilon}$ <sup>d</sup> [mm s <sup>-1</sup> ]	H <sup>e</sup> [T]	$\sigma_{\text{H}}$ <sup>d</sup> [T]	Area [%]	Red. $\chi^2$ <sup>f</sup>
$^{57}\text{Fe}$ -Lp (5 K)	3	RF – anoxic	D1 – Fe(III)	0.43	0.96	0.62	-	-	6.9	0.95
			D2 – Fe(II)	1.26	2.30	0.35	-	-	2.5	
			S1 – Fh	0.47*	-0.01*	0.19*	48.84*	2.74*	34.7	
			S2 – Lp	0.47	0.005*	-	42.78	3.0	24.6	
			H1				45.0	1.5		
			H2				42.0	3.0		
			Frac. H2				75%			
			S3 – Gt	0.49	-0.12	-	49.96	1.09	25.4	
			CF	1.00*	0.00*	-	26.60*	19.20*	5.8	
			4	RF – oxic	D1 – Fe(III)	0.49	0.83	0.39	-	
D2 – Fe(II)	1.26	2.70*			0.80*	-	-	1.3		
S1 – Fh	0.47*	-0.01*			0.19*	48.84*	2.74*	36.7		
S2 – Lp	0.48	0.005*			-	43.05	2.95	21.9		
H1						45.0	1.5			
H2						42.0	3.0			
Frac. H2						64%				
S3 – Gt	0.49	-0.13			-	49.92	0.96	24.9		
CF	0.5*	0.00*			-	26.60*	19.20*	9.8		
7	RF – anoxic	D1 – Fe(III)			0.47*	0.98	0.55	-	-	11.1
		D2 – Fe(II)	1.21	2.85	0.95	-	-	10.9		
		S1 – Fh	0.47*	-0.01*	0.19*	48.84*	2.74*	12.9		
		S2 – Lp	0.47*	0.005*	-	42.94	2.97	11.2		
		H1				45.0	1.5			
		H2				42.0	3.0			
		Frac. H2				69%				
		S3 – Gt	0.48	-0.11	-	49.90	0.94	48.2		
		CF	1.00*	0.00*	-	26.60*	19.20*	5.4		

Table S10: continued.

Sample	Time [week]	Type	Fit c.	CS <sup>a</sup> [mm s <sup>-1</sup> ]	QS <sup>b</sup> or $\epsilon^c$ [mm s <sup>-1</sup> ]	$\sigma_{QS}$ or $\sigma_\epsilon^d$ [mm s <sup>-1</sup> ]	H <sup>e</sup> [T]	$\sigma_H^d$ [T]	Area [%]	Red. $\chi^{2f}$
<sup>57</sup> Fe-Lp (5 K)	8	RF – oxic	D1 – Fe(III)	0.47	0.81	0.44	-	-	8.7	0.59
			D2 – Fe(II)	1.20*	2.80*	0.80*	-	-	1.6	
			S1 – Fh	0.47*	-0.01*	0.19*	48.84*	2.74*	29.0	
			S2 – Lp	0.44	0.005*	-	42.04	2.95	14.7	
			H1				45.0	1.5		
			H2				42.0	3.0		
			Frac H2				65%			
			S3 – Gt	0.48	-0.13	-	49.98	0.70	34.3	
			CF	0.50*	0.00*	-	26.60*	19.20*	11.7	
			11	RF – anoxic	D1 – Fe(III)	0.50*	0.80*	0.40*	-	
D2 – Fe(II)	1.27	2.76			0.50*	-	-	17.3		
S1 – Fh	0.47*	-0.01*			0.19*	48.84*	2.74*	12.1		
S2 – Lp	-	-			-	-	-	0.0		
S3 – Gt	0.48	-0.13			-	49.64	0.54	45.2		
CF	1.00*	0.00*			-	26.60*	19.20*	22.3		
12	RF – oxic	D1 – Fe(III)			0.43	0.75	0.42	-	-	8.9
		D2 – Fe(II)	1.20*	2.70*	0.80*	-	-	1.8		
		S1 – Fh	0.47*	-0.01*	0.19*	48.84*	2.74*	22.7		
		S2 – Lp	0.51	0.005*	-	43.30	2.88	6.4		
		H1				45.00	1.50			
		H2				42.00	3.00			
		Frac H2				57%				
		S3 – Gt	0.48	-0.13	-	49.97	0.78	45.2		
CF	0.50*	0.00*	-	26.60*	19.20*	15.0				

Table S10: continued.

Sample	Time [week]	Type	Fit c.	CS <sup>a</sup> [mm s <sup>-1</sup> ]	QS <sup>b</sup> or $\epsilon$ <sup>c</sup> [mm s <sup>-1</sup> ]	$\sigma_{QS}$ or $\sigma_{\epsilon}$ <sup>d</sup> [mm s <sup>-1</sup> ]	H <sup>e</sup> [T]	$\sigma_H$ <sup>d</sup> [T]	Area [%]	Red. $\chi^2$ <sup>f</sup>
<sup>57</sup> Fe-Lp (5 K)	12	PF – anoxic	D1 – Fe(III)	0.50*	0.80*	0.40*	-	-	5.9	1.10
			D2 – Fe(II)	1.26	2.93	0.50*	-	-	21.6	
			S1 – Fh	0.47*	-0.01*	0.19*	48.84*	2.74*	9.7	
			S2 – Lp	0.47*	0.005*	-	42.00	3.00	1.4	
			S3 – Gt	0.47	-0.12	-	49.83	0.60	34.1	
			CF	0.80*	0.00*	-	26.60*	19.20*	26.6	

<sup>a</sup> CS, Center shift;

<sup>b</sup> QS, Quadrupole splitting (for doublets);

<sup>c</sup>  $\epsilon$ , Quadrupole shift (for sextets);

<sup>d</sup>  $\sigma$ , standard deviation of QS,  $\epsilon$  or H;

<sup>e</sup> H, Hyperfine field;

<sup>f</sup> Reduced  $\chi^2$ , goodness of fit;

\* Indicates values that were fixed during the fitting process.

Abbreviations: RF = redox fluctuating mesocosms, PF = permanently flooded mesocosm, D = doublet, S = sextet, Fh = ferrihydrite, Lp = lepidocrocite, Gt = goethite, CF = collapsed feature.

Fitting parameters (5 K) of <sup>54</sup>Fe-mineral samples**Table S11:** Mössbauer fitting parameters for spectra collected from initial and incubated <sup>54</sup>Fe ferrihydrite (<sup>54</sup>Fe-Fh) at 5 K. M1 and M2 refer to magnetite sextets with parameters derived from Doriguetto et al.<sup>25</sup>

Sample	Time [week]	Type	Component	CS <sup>a</sup> [mm s <sup>-1</sup> ]	ε <sup>b</sup> [mm s <sup>-1</sup> ]	σ <sub>ε</sub> <sup>c</sup> [mm s <sup>-1</sup> ]	H <sup>d</sup> [T]	σ <sub>H</sub> <sup>c</sup> [T]	Area [%]	Red. χ <sup>2e</sup>
<sup>54</sup> Fe-Fh (5 K)	11	RF – anoxic	S1+3 – Fh + Gt	0.48	-0.13	-	49.75	0.8	53.5	1.17
			M1	0.47	0.05	0.1*	50.91	1.5*	37.2	
			M2	0.85*	-0.26	0.1*	46.91	1.5*	9.3	
	12	RF – oxic	S1+3 - Fh + Gt	0.48	-0.13	-	49.87	0.77	43.2	1.94
			M1	0.46	0.02	0.1*	51.77	1.5*	49.6	
			M2	0.85*	-0.33	0.1*	46.77	1.5*	7.23	
	12	PF – anoxic	S1+3 - Fh + Gt	0.48	-0.12	-	49.92	0.77	50.7	8.07
			M1	0.42	0.05	0.1*	51.04	1.5*	31.7	
			M2	0.85*	-0.33	0.1*	47.25	1.5*	17.61	

<sup>a</sup> CS, Center shift;<sup>b</sup> QS, Quadrupole splitting (for doublets);<sup>c</sup> ε, Quadrupole shift (for sextets);<sup>d</sup> σ, standard deviation of QS, ε or H;<sup>e</sup> H, Hyperfine field;<sup>f</sup> Reduced χ<sup>2</sup>, goodness of fit;

\* Indicates values that were fixed during the fitting process.

Abbreviations: RF = redox fluctuating mesocosms, PF = permanently flooded mesocosm, Fh = ferrihydrite, Gt = goethite, S = sextet, M = magnetite sextet.

**Table S12:** Mössbauer fitting parameters for spectra collected from initial and incubated  $^{54}\text{Fe}$  lepidocrocite ( $^{54}\text{Fe}$ -Lp) at 5 K. M1 and M2 refer to magnetite sextets with parameters derived from Doriguetto et al.<sup>25</sup>

Sample	Time [week]	Type	Component	CS <sup>a</sup> [mm s <sup>-1</sup> ]	$\varepsilon$ <sup>b</sup> [mm s <sup>-1</sup> ]	$\sigma_{\varepsilon}$ <sup>c</sup> [mm s <sup>-1</sup> ]	H <sup>d</sup> [T]	$\sigma_H$ <sup>e</sup> [T]	Area [%]	Red. $\chi^2$ <sup>e</sup>
$^{54}\text{Fe}$ -Lp (5 K)	11	RF – anoxic	S1+3 - Fh + Gt	0.48	0.02	-	44.44	1.2*	55.8	7.17
			M1	0.44	-0.01	0.1*	50.83	1.2*	34.9	
			M2	0.85*	-0.36	0.1*	47.73	1.2*	9.3	
	12	RF – oxic	S1+3 - Fh + Gt	0.46	0.01	-	44.28	1.2*	35.9	5.8
			M1	0.42	0.00	0.1*	51.51	1.2*	46.8	
			M2	0.85*	-0.38	0.1*	48.13	1.2*	17.3	
	12	PF – anoxic	S1+3 - Fh + Gt	0.50	0.01	-	44.65	1.2*	48.5	1.29
			M1	0.42	-0.02	0.1*	51.03	1.2*	37.1	
			M2	0.85*	-0.37	0.1*	48.04	1.2*	14.1	

<sup>a</sup> CS, Center shift;<sup>b</sup> QS, Quadrupole splitting (for doublets);<sup>c</sup>  $\varepsilon$ , Quadrupole shift (for sextets);<sup>d</sup>  $\sigma$ , standard deviation of QS,  $\varepsilon$  or H;<sup>e</sup> H, Hyperfine field;<sup>f</sup> Reduced  $\chi^2$ , goodness of fit;

\* Indicates values that were fixed during the fitting process.

Abbreviations: RF = redox fluctuating mesocosms, PF = permanently flooded mesocosm, Fh = ferrihydrite, Gt = goethite, S = sextet, M = magnetite sextet.

**S12. Comparison of iron mineral fractions determined by different methods**

The XRD, Fe K-edge XAS and Mössbauer analyses identified the same main mineral phases and similar mineral fractions in the samples (Table S13). Ferrihydrite fractions quantified by XRD using the PONKCS approach<sup>6</sup> were slightly higher than fractions quantified by linear combination fitting of Fe K-edge EXAFS spectra. Magnetite fractions quantified by Mössbauer spectroscopy were generally higher than in XRD and XAS results. However, magnetite fitting in Mössbauer spectra is challenging at low temperature, since magnetite contributes up to five overlapping sextets to Mössbauer spectra at 5 K<sup>25</sup> (Figure S19). This may explain the potential overestimation of magnetite fractions by Mössbauer. Further, in Mössbauer spectra of <sup>57</sup>Fe-ferrihydrite samples we did not differentiate between ferrihydrite and goethite, since the magnetite sextets strongly overlap with sextets of ferrihydrite and goethite (Figure S19).

**Table S13:** Mineral fractions in the <sup>57</sup>Fe-mineral samples without soil, incubated for 11 and 12 weeks in the redox fluctuating mesocosms (RF) and for 12 weeks in the permanently flooded mesocosm (PF), analyzed by X-ray diffraction (XRD), linear combination fitting of Fe K-edge EXAFS spectra (Fe EXAFS) and Mössbauer spectroscopy. Mineral fractions quantified by XRD are normalized to the number of Fe atoms in the respective mineral crystal structure (Fh = (Fe<sup>3+</sup>)<sub>2</sub>O<sub>3</sub>•0.5H<sub>2</sub>O; Lp = FeOOH; Gt = FeOOH; Mt = Fe<sub>3</sub>O<sub>4</sub>, Sd = FeCO<sub>3</sub>). Abbreviations: w = week, Fh = ferrihydrite, Lp = lepidocrocite, Gt = goethite, Mt = magnetite, Sd = siderite.

Mineral	Technique	Time [w]	Treatment	Fh	Lp	Gt	Mt	Sd
<sup>57</sup> Fe-Ferrihydrite	XRD	11	RF – anoxic	38	-	36	23	3
		12	RF – oxic	38	-	30	30	2
		12	PF – anoxic	33	-	34	29	3
	Fe EXAFS	11	RF – anoxic	17	-	51	32	-
		12	RF – oxic	31	-	38	31	-
		12	PF – anoxic	6	-	48	46	-
	Mössbauer (5 K)	11	RF – anoxic	-	-	54*	46	-
		12	RF – oxic	-	-	43*	57	-
		12	PF – anoxic	-	-	51*	49	-
<sup>57</sup> Fe-Lepidocrocite	XRD	11	RF – anoxic	-	65	-	32	4
		12	RF – oxic	-	48	-	50	2
		12	PF – anoxic	-	54	-	45	1
	Fe EXAFS	11	RF – anoxic	-	89	-	11	-
		12	RF – oxic	-	72	-	28	-
		12	PF – anoxic	-	70	-	30	-
	Mössbauer (5 K)	11	RF – anoxic	-	56	-	44	-
		12	RF – oxic	-	36	-	64	-
		12	PF – anoxic	-	49	-	51	-

\*this fraction may also contain ferrihydrite.

## References

- 1 C. Chen and A. Thompson, The influence of native soil organic matter and minerals on ferrous iron oxidation, *Geochim. Cosmochim. Acta*, 2021, **292**, 254–270.
- 2 J. M. Byrne and A. Kappler, A revised analysis of ferrihydrite at liquid helium temperature using Mössbauer spectroscopy, *Am. Mineral.*, 2022, **107**, 1643–1651.
- 3 S. W. Poulton and D. E. Canfield, Development of a sequential extraction procedure for iron: Implications for iron partitioning in continentally derived particulates, *Chem. Geol.*, 2005, **214**, 209–221.
- 4 J. M. Byrne and A. Kappler, in *Analytical Geomicrobiology: A Handbook of Instrumental Techniques*, Cambridge University Press, Cambridge, 2019, pp. 314–338.
- 5 D. L. Bish and S. A. Howard, Quantitative phase analysis using the Rietveld method, *J. Appl. Crystallogr.*, 1988, **21**, 86–91.
- 6 N. V. Y. Scarlett and I. C. Madsen, Quantification of phases with partial or no known crystal structures, *Powder Diffr.*, 2006, **21**, 278–284.
- 7 M. Aeppli, R. Kaegi, R. Kretzschmar, A. Voegelin, T. B. Hofstetter and M. Sander, Electrochemical analysis of changes in iron oxide reducibility during abiotic ferrihydrite transformation into goethite and magnetite, *Environ. Sci. Technol.*, 2019, **53**, 3568–3578.
- 8 L. K. ThomasArrigo, J. M. Byrne, A. Kappler and R. Kretzschmar, Impact of organic matter on iron(II)-catalyzed mineral transformations in ferrihydrite–organic matter coprecipitates, *Environ. Sci. Technol.*, 2018, **52**, 12316–12326.
- 9 K. Schulz, L. K. ThomasArrigo, R. Kaegi and R. Kretzschmar, Stabilization of ferrihydrite and lepidocrocite by silicate during Fe(II)-catalyzed mineral transformation: Impact on particle morphology and silicate distribution, *Environ. Sci. Technol.*, 2022, **56**, 5929–5938.
- 10 A. P. Zhukhlistov, Crystal structure of lepidocrocite FeO(OH) from the electron-diffractometry data, *Crystallogr. Reports*, 2001, **46**, 730–733.
- 11 E. Zepeda-Alarcon, H. Nakotte, A. F. Gualtieri, G. King, K. Page, S. C. Vogel, H.-W. Wang and H.-R. Wenk, Magnetic and nuclear structure of goethite ( $\gamma$ -FeOOH): a neutron diffraction study, *J. Appl. Crystallogr.*, 2014, **47**, 1983–1991.
- 12 M. E. Fleet, The structure of magnetite, *Acta Crystallogr. Sect. B*, 1981, **37**, 917–920.
- 13 B. Lavina, P. Dera, R. T. Downs, W. Yang, S. Sinogeikin, Y. Meng, G. Shen and D. Schiferl, Structure of siderite FeCO<sub>3</sub> to 56 GPa and hysteresis of its spin-pairing transition, *Phys. Rev. B*, 2010, **82**, 64110.
- 14 W. A. Dollase, Correction of intensities for preferred orientation in powder diffractometry: application of the March model, *J. Appl. Crystallogr.*, 1986, **19**, 267–272.
- 15 C. A. Gorski and M. M. Scherer, Determination of nanoparticulate magnetite stoichiometry by Mössbauer spectroscopy, acidic dissolution, and powder X-ray diffraction: A critical review, *Am. Mineral.*, 2010, **95**, 1017–1026.
- 16 R. M. Cornell and U. Schwertmann, *The iron oxides*, Wiley, Weinheim, Germany, 2003.
- 17 B. Ravel and M. Newville, ATHENA, ARTEMIS, HEPHAESTUS: Data analysis for X-ray absorption spectroscopy using IFFFIT, *J. Synchrotron Radiat.*, 2005, **12**, 537–541.
- 18 C. M. Hansel, S. G. Benner and S. Fendorf, Competing Fe(II)-induced mineralization pathways of ferrihydrite, *Environ. Sci. Technol.*, 2005, **39**, 7147–7153.

- 19 C. M. Hansel, S. G. Benner, J. Neiss, A. Dohnalkova, R. K. Kukkadapu and S. Fendorf, Secondary mineralization pathways induced by dissimilatory iron reduction of ferrihydrite under advective flow, *Geochim. Cosmochim. Acta*, 2003, **67**, 2977–2992.
- 20 P. Langner, C. Mikutta and R. Kretzschmar, Arsenic sequestration by organic sulphur in peat, *Nat. Geosci.*, 2012, **5**, 66–73.
- 21 S. D. Kelly, D. Hesterberg and B. Ravel, in *Ulery, A.L., Drees, L.R. (Eds.), Methods of Soil Analysis. Part 5. Mineralogical Methods. Soil Society of America, Madison*, 2015, pp. 387–463.
- 22 E. J. O’Loughlin, M. I. Boyanov, C. A. Gorski, M. M. Scherer and K. M. Kemner, Effects of Fe(III) oxide mineralogy and phosphate on Fe(II) secondary mineral formation during microbial iron reduction, *Minerals*, 2021, **11**, 1–43.
- 23 M. Egger, T. Jilbert, T. Behrends, C. Rivard and C. P. Slomp, Vivianite is a major sink for phosphorus in methanogenic coastal surface sediments, *Geochim. Cosmochim. Acta*, 2015, **169**, 217–235.
- 24 D. G. Rancourt and J. Y. Ping, Voigt-based methods for arbitrary-shape static hyperfine parameter distributions in Mössbauer spectroscopy, *Nucl. Inst. Methods Phys. Res. B*, 1991, **58**, 85–97.
- 25 A. C. Doriguetto, N. G. Fernandes, A. I. C. Persiano, E. N. Filho, J. M. Grenèche and J. D. Fabris, Characterization of a natural magnetite, *Phys. Chem. Miner.*, 2003, **30**, 249–255.
- 26 A. Thompson, D. G. Rancourt, O. A. Chadwick and J. Chorover, Iron solid-phase differentiation along a redox gradient in basaltic soils, *Geochim. Cosmochim. Acta*, 2011, **75**, 119–133.
- 27 P. Winkler, K. Kaiser, A. Thompson, K. Kalbitz, S. Fiedler and R. Jahn, Contrasting evolution of iron phase composition in soils exposed to redox fluctuations, *Geochim. Cosmochim. Acta*, 2018, **235**, 89–102.
- 28 E. E. Daugherty, B. Gilbert, P. S. Nico and T. Borch, Complexation and Redox Buffering of Iron(II) by Dissolved Organic Matter, *Environ. Sci. Technol.*, 2017, **51**, 11096–11104.
- 29 T. Frederichs, T. von Döbeneck, U. Bleil and M. J. Dekkers, Towards the identification of siderite, rhodochrosite, and vivianite in sediments by their low-temperature magnetic properties, *Phys. Chem. Earth, Parts A/B/C*, 2003, **28**, 669–679.
- 30 H. C. Meijer, J. Van den Handel and E. Frikkee, Magnetic behaviour of vivianite,  $\text{Fe}_3(\text{PO}_4)_2 \cdot 2\text{H}_2\text{O}$ , *Physica*, 1967, **34**, 475–483.
- 31 L. Notini, K. Schulz, L. J. Kubeneck, A. R. C. Grigg, K. A. Rothwell, G. Fantappiè, L. K. Thomas-Arrigo and R. Kretzschmar, A new approach for investigating iron mineral transformations in soils and sediments using  $^{57}\text{Fe}$ -labeled minerals and  $^{57}\text{Fe}$  Mössbauer spectroscopy, *Environ. Sci. Technol.*, 2023, **57**, 10008–10018.